Upconverting nanoparticles in aqueous media: not a dead-end road. Avoiding degradation by using hydrophobic polymer shells

Diego Mendez-Gonzalez,* Vivian Torres Vera, Irene Zabala Gutierrez, Concepción Cascales, Jorge Rubio-Retama, Oscar G. Calderón, Sonia Melle,* Marco Laurenti.*

Dr. D. Mendez-Gonzalez, V. T. Vera, I. Z. Gutierrez, Prof. J. Rubio-Retama, Prof. M. Laurenti. Department of Chemistry in Pharmaceutical Sciences, Complutense University of Madrid, E-28040 Madrid, Spain. E-mail: diegomen@ucm.es ; marclaur@ucm.es

Dr. Mendez-Gonzalez. Nanomaterials for Bioimaging Group (nanoBIG), Departamento de Física de Materiales, Facultad de Ciencias, Universidad Autónoma de Madrid, C/ Francisco Tomás y Valiente 7, Madrid 28049, Spain.

Dr. D. Mendez-Gonzalez, Prof. J. Rubio-Retama, Prof. M. Laurenti. Nanobiology Group, Instituto Ramón y Cajal de Investigación, Sanitaria Hospital Ramón y Cajal, Ctra. De Colmenar Viejo, Km. 9,100, 28034 Madrid, Spain

Prof. C. Cascales. Instituto de Ciencia de Materiales de Madrid, Consejo Superior de Investigaciones Científicas CSIC, c/Sor Juana Inés de la Cruz, 28049, Madrid, Spain.

Prof. S. Melle, Prof. O. G. Calderón. Department of Optics, Complutense University of Madrid, E-28037 Madrid, Spain. E-mail: smelle@fis.ucm.es

Upconverting nanoparticles in aqueous media: not a dead-end road. Avoiding degradation by using hydrophobic polymer shells.

Diego Mendez-Gonzalez, Vivian Torres Vera, Irene Zabala Gutierrez, Concepción Cascales, Jorge Rubio-Retama, Oscar G. Calderón, Sonia Melle,* Marco Laurenti.**

Keywords: upconversion nanoparticles, polymers, shell, dissolution, degradation, phosphate, protection

Abstract

The stunning optical properties of upconverting nanoparticles (UCNPs) have inspired promising and unique biomedical technologies. However, as a necessary step for their use in bio-applications, their transfer to aqueous media is accompanied by highly detrimental effects. Namely, intense luminescence quenching and partial dissolution by water, as well as complete degradation by other molecules such as phosphates. Whereas the translation of UCNPs to the medical market would open new and interesting avenues for ultrasensitive diagnostics and other medical technologies, their concentration- and time-dependent degradation currently challenges the realistic bio-application of these nanomaterials. In this work, we developed a strategy to protect UCNPs by creating an isolating hydrophobic polymer shell (HPS) through miniemulsion polymerization. Stability studies revealed that these HPS served as a very effective barrier, impeding polar molecules to affect UCNP's optical properties. Even more, it allowed UCNPs to withstand even extremely aggressive conditions such as very high dilutions, high phosphate concentrations, and high temperatures. In-depth optical, morphological, and atomic-level chemical characterization proved the potential of HPS to overcome the current limitations of UCNPs. This strategy, which can be applicable to other nanomaterials with similar limitations, pave the way towards more stable and reliable UCNPs with expanded applications in life sciences.

1. Introduction

Lanthanide-doped upconverting nanoparticles (UCNPs) probably feature one of the most distinctive and stable emissions among photoluminescent materials.[1] Arising from the sequential absorption of two or more low energy photons and the subsequent emission of a fewer number of higher energy photons, photon upconversion is accompanied by large anti-

Stokes shifts and lack of autofluorescence from the surrounding biomolecules. As a result, long-lived and background-free emissions are obtained. In combination with the absence of blinking and their remarkable photostability, these properties make UCNPs ideal luminescent probes for applications within biological media.[2] Lanthanide-doped UCNPs based on fluoride matrices (e.g., β-$NaYF_4$, β-$NaGdF_4$) are currently the most widely used nanomaterials sustaining photon upconversion processes between lanthanides such as Yb^{3+} and Er^{3+}, as these matrices allow the best quantum efficiencies due to their inherent low phonon energies.[3–5] Nevertheless, most of these UCNPs must be transferred to aqueous media (e.g., biological fluids, buffers) in order to be effectively used as luminescent probes in bio-applications such as sensing, imaging, *in vitro* or *in vivo* nano-thermometry, or as light converters to trigger local photochemical reactions in biological environments.[6–11] Unfortunately, this mandatory transfer step to water is highly detrimental to their luminescent properties, and therefore, for their realistic bio-applications due to several reasons.[6–8,12] First, the aqueous transfer of UCNPs is normally accompanied by an intense reduction of their lifetime and luminescence of their constituent lanthanides.[13,14] This is in part due to a surface quenching that stems from the vibrational modes of the hydrophilic molecules used to turn UCNPs water-dispersible, but mostly due to a combination of the strong non-radiative relaxation of Yb^{3+} when coupled with water vibrational modes, and the relatively high absorption by water of the wavelength used to excite Yb^{3+}-sensitized UCNPs' (i.e. 980 nm).[13,14] Second, the solubility equilibrium of UCNPs' matrices like β-$NaYF_4$, one of the most efficient and commonly used hosts, is quite low (1.6×10^{-26}).[15] However, the high specific surface area of UCNPs (~4.64 m^2/g for UNCPs of $\emptyset$ = 30 nm), together with the low concentrations normally required in bio-applications, are in such ranges that UCNPs often suffer time-dependent structural degradation, due to dissolution-reprecipitation of their host matrices until reaching solubility equilibrium with the surrounding aqueous media.[16,17] In fact, this effect over the UCNPs' structural integrity has been reported for concentrations lower than 50 μg/mL in nanoparticles with diameters of 25-31 nm.[15] In this regard, it is reasonable to think that this phenomenon will have an even more deleterious effect in the new generations of UCNPs, given the current trend of synthesizing ultra-small UCNPs for biological applications, or designing core/shell UCNPs, where the dissolution of the shells that are used to improve their quantum efficiencies or change their optical properties will result in an important reduction of their luminescence and a change in their optical features.[18–22] On top of that, increasing the temperature of the medium shifts the solubility equilibrium towards the dissolution of UCNPs to an even higher extent. Because of this, the application of UCNPs in fields such as nano-thermometry or platforms that require thermal cycles such as Polymer Chain Reaction (PCR)

is currently very hampered when low concentrations of UCNPs are required. Third, the fact that fluoride (F^-) and lanthanide ions (Ln^{3+}) are released to the aqueous medium until reaching the solubility equilibrium has important implications. On the one hand, the presence of chemical species that can capture free Ln^{3+} and form more stable compounds compared with the original host matrices will displace the solubility equilibrium of the matrices until the complete dissolution of UCNPs occurs. This is the case of phosphates (e.g., phosphate buffers), but also of different compounds and buffers that have proven to harm UCNPs and irreversibly affect their luminescent properties.[23,24] On the other hand, the presence of F^- and Ln^{3+} ions in solution raise some questions and concerns about the biocompatibility and bioaccumulation of these ions when using UCNPs in biological fluids. As an example, several toxicity issues have already been ascribed to F^- and Ln^{3+}.[25–30] Besides, the high phosphate content at specific locations within the body, such as the bones' mineral matrix, may be prone to bioaccumulate Ln^{3+} when using UCNPs *in vivo*.[29,31]

These drawbacks urge to develop a strategy that satisfactorily solves these limitations, giving a step forward to ensure realistic prospects for these promising materials in life sciences, while expanding their range of current possible applications. In this direction, different approaches have been explored to alleviate some of these problems. For example, Lahtinen et al. took advantage of the so-called common ion effect (adding KF to aqueous solutions) to hamper dissolution of UCNPs when used at low concentrations and room temperature (RT).[15] In a later work, Palo et al. developed a strategy based on the coating of UCNPs with oppositely charged polyelectrolyte bilayers to delay the disintegration of UCNPs, especially during the first 5 hours.[32] A similar layer by layer strategy was used later to help alleviating the quenching exerted by water molecules.[33] In other works, ligand exchange of UCNP's capping agent by a proper molecule has also proven, in some cases, to hamper this luminescence quenching.[34] Interestingly, when some phosphate/phosphonate-containing molecules are used in this kind of ligand exchange strategies, the resulting UCNPs seem to show enhanced resistance to chemically harmful molecules such as phosphate buffer and acidic media.[30,33,35] This is explained by the high binding affinity between phosphonate moieties and the Ln^{3+} located at the surface of UCNPs, which hampers the release of ions from the host matrix and partially shields against other ligands and water molecules. Nevertheless, not all phosphonates passivate UCNPs' surface effectively.[36] In fact, literature seems to indicate that passivation is often increased by capping agents that simultaneously combine one or more phosphonate/phosphonic groups in one side, which strongly coordinates to the UCNPs' surface, and a less polar moiety (e.g. or aliphatic chains) on the other side to provide shielding from water and other

ligands.[30,37–39] Interestingly, using capping agents that contain carboxylic or sulfonate groups instead of phosphonate moieties, or just preserving the UCNPs' original capping agents (e.g. oleic acid), seem viable strategies to partially protect UCNPs from the surrounding aqueous environment as long as these are coated with amphipathic molecules with long aliphatic chains or polymer chains with reduced polarity.[39–42] This highlights the importance of creating a relatively robust and effective shielding layer surrounding the UCNPs, as this seems to partially limit the diffusion of water and other possible ligands that are capable to exert detrimental effects on the optical properties and structural integrity of UCNPs. In fact, the use of an intermediate shielding layer with hydrophobic properties may be one of the best possible approaches, as not only it would contribute to keeping away polar and harmful molecules from diffusing towards the surface of UCNPs, but it should partially maintain a local environment resembling the original post-synthetic hydrophobic conditions (e.g., chloroform or hexane dispersions) where UCNPs exhibit their best performances. Bearing all this in mind and based on the lack of just a single strategy that simultaneously addresses all the aforementioned drawbacks in a general and less situational manner (i.e., serving potentially for *in vitro*, *in vivo*, and both room temperature (RT) and high temperature applications), we present a simple and rationale design of the UCNPs' surface that ensures their protection in aqueous media under different harsh conditions.

Our approach is based on the combination of two synergic strategies: First, the oleic acid ligands at the surface of UCNPs are replaced in non-polar solvents by 10-methacryloyldecylphosphate (MDP), to achieve surface passivation, colloidal stability in organic media, and a terminal polymerizable group. Second, the dispersion and free-radical miniemulsion polymerization of these UCNPs in styrene, or a mixture of styrene (St) and methyl methacrylate (MMA), pursues the formation of a robust hydrophobic shell of controlled thickness that insulates and protects UCNPs from aqueous environment. This method is also expected to provide them with colloidal stability in aqueous media due to the presence of polar groups incorporated during the polymerization process. Full optical, morphological, and chemical characterization of the resulting polymer-coated UCNPs was carried out, and their resistance to different harsh conditions such as phosphate buffer, very high dilutions, and high temperatures was studied. A stunning improvement in UCNPs' chemical resistance is proved, suggesting that this kind of strategy may pave the way towards safer UCNPs with more reliable optical properties and expanded applications in life sciences.

2. Results and discussion

2.1. Synthesis of UCNPs and functionalization with MDP

The synthesis of β-$NaYF_4$:$Yb_{0.20}$,$Er_{0.02}$ was performed according to a previous thermal co-precipitation method.[43] The adapted protocol described in the methods section of the Supporting Information yielded monodisperse UCNPs. The mean diameter of the synthesized UCNPs used in this work was 36 ± 1 nm. A representative TEM picture of the resulting β-$NaYF_4$:$Yb_{0.20}$,$Er_{0.02}$ UCNPs is depicted in Supporting Information (Figure S1A), showing their monodisperse size distribution and quasi-spherical morphology. HR-TEM analyses (Figure S1B) shows the crystalline structure of the synthesized UCNPs, with a characteristic lattice distance of 0.52 nm that can be assigned to (100) lattice plane of the hexagonal beta phase of $NaYF_4$.[44] SAED analysis further confirmed that $NaYF_4$:$Yb_{0.20}$,$Er_{0.02}$ UCNPs were in their β-phase according to the JCPDS 16-0334 diffraction card (Figure S1C).

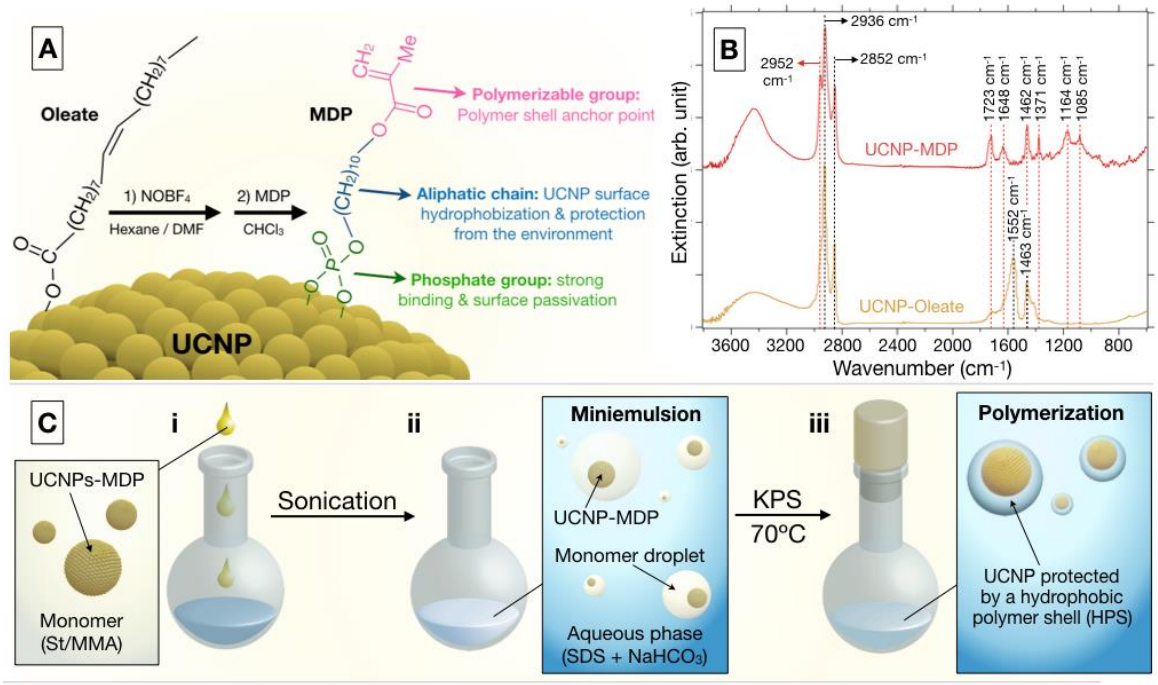

Scheme 1. A) UCNPs' surface functionalization process involving 1) the removal of oleate capping agent with $NOBF_4$ and 2) the functionalization of UCNPs with MDP in $CHCl_3$. B) FT-IR spectra of the UCNPs capped with oleate and MDP. C) Main steps required to coat UCNPs-MDP with the HPS through miniemulsion polymerization. Namely, i) dropwise addition of UCNPs-MDP dispersed in the monomer (St or St/MMA mixtures) onto the aqueous phase containing SDS and $NaHCO_3$; ii) ultrasonication of the mixture to produce the nanodroplets (i.e., miniemulsion); iii) addition of radical initiator (KPS) and initiation of the polymerization by heating at 70 ºC.

The subsequent treatment of UCNPs with $NOBF_4$ removed from their surface the oleate molecules, which acted as capping agent, allowing the phase transfer of the resulting UCNPs from hexane to DMF. Their later incubation with MDP in DMF/$CHCl_3$ resulted in their surface functionalization with MDP, as demonstrated by FT-IR analyses (see Scheme 1A and 1B). FTIR analyses of the initial oleate-capped UCNPs yielded the characteristic peaks from the asymmetric and symmetric stretching vibrations of the COO^- group at 1463 cm^{-1} and 1552 cm^{-1}, respectively.[45,46] The additional peaks present at 2852 cm^{-1} and 2936 cm^{-1} correspond to the symmetric and asymmetric stretching vibrations of the oleate aliphatic chain, respectively.[45] Interestingly, after completing the process of ligand exchange with MDP, major changes in the FTIR spectra of UCNPs can be observed: I) New peaks appear at 1085 cm^{-1} and 1164 cm^{-1} corresponding to the P=O stretching vibration, when substituted with –O, and the in-phase stretch vibration of the $P\text{-}O^-$, II) the peaks at 1648 cm^{-1} and 1723 cm^{-1} evidence the presence of the methacryloyl moiety within the MDP, as these correspond to the stretching vibration of C=C conjugated to carbonyl groups and of C=O conjugated groups, respectively, III) the peaks at 2852 cm^{-1}, 2936 cm^{-1}, and 2952 cm^{-1} are assigned to the symmetric and asymmetric CH_2 stretching, and the CH_2-O asymmetric stretching from the ether within MDP, respectively.[45] The ligand exchange with MDP provides the resulting UCNPs with several advantages, see Scheme 1A. First, the phosphate group within MDP has a strong binding affinity towards the surface of UCNPs,[35] ensuring that the ligand does not detach easily, while providing surface passivation. Second, the MDP aliphatic chain provides hydrophobicity to the surface, which allows UCNPs to be dispersed in the hydrophobic monomer precursors (i.e., styrene and methyl methacrylate) that will be polymerized to yield the protective polymer shell in later steps. The MDP aliphatic chains also hamper the adsorption of polar molecules onto the UCNPs surface, minimizing the luminescence quenching produced by water. Third, the MDP methacryloyl moiety will provide a starting point to initiate, propagate or terminate the growth of polymer chains during the formation of the protective polymer shell. Finally, MDP can also improve the wetting of UCNPs with polystyrene and other hydrophobic polymers, favoring a more homogeneous growth of the polymer shell barrier around them and a complete coating of their surface.

2.2. Coating of UCNPs with HPS by miniemulsion polymerization.

Miniemulsion polymerization was used to coat the resulting UCNPs-MDP with a protective HPS. In this method, St, or a mixture of St and MMA, formed the dispersed oily phase; sodium dodecyl sulfate (SDS) was used as surfactant; hexadecane was used as hydrophobe or droplet

co-stabilizer; and potassium persulfate (KPS) was used as the radical initiator.[47,48] Miniemulsion polymerization was chosen as the coating method since it offers several advantages compared with other polymerization approaches such as fast polymerization kinetics, high St conversions, the possibility to encapsulate single or multiple NPs thanks to their isolation in monomer nanodroplets (i.e. nanoreactors), and a relatively easy control of the polymer shell composition, thickness and morphology.[47–52]

Interestingly, if oleate-capped UCNPs are directly used in this polymerization process, uncoated snowman-like Janus structures are obtained, due to the partial phase separation between the polymer shell and the nanoparticle during polymerization (see Figure S2). This was one of the reasons to substitute oleate by a potentially more suitable moiety such as MDP. The coating of UCNPs-MDP by miniemulsion polymerization is summarized in Scheme 1C. First, UCNPs-MDP were dispersed in St or St/MMA mixtures, and added dropwise to a vigorously stirred aqueous solution of 40 mM SDS and 1.2 mM $NaHCO_3$, see Scheme 1C-i. After stirring for 1 h, the resulting emulsion was ultrasonicated, in order to reduce the size of the monomer droplets down to the nanometric range, see Scheme 1C-ii. This allows to create independent nanoreactors containing the UCNPs-MDP, where the polymerization can start in parallel to encapsulate the UCNPs contained thereof.[49] After heating the solution to 70 ^{o}C, KPS was added to start the radical polymerization of the monomer droplets, yielding the polystyrene (PS) or poly-styrene-co-poly-methyl methacrylate (PS/PMMA) HPS, see Scheme 1C-iii.

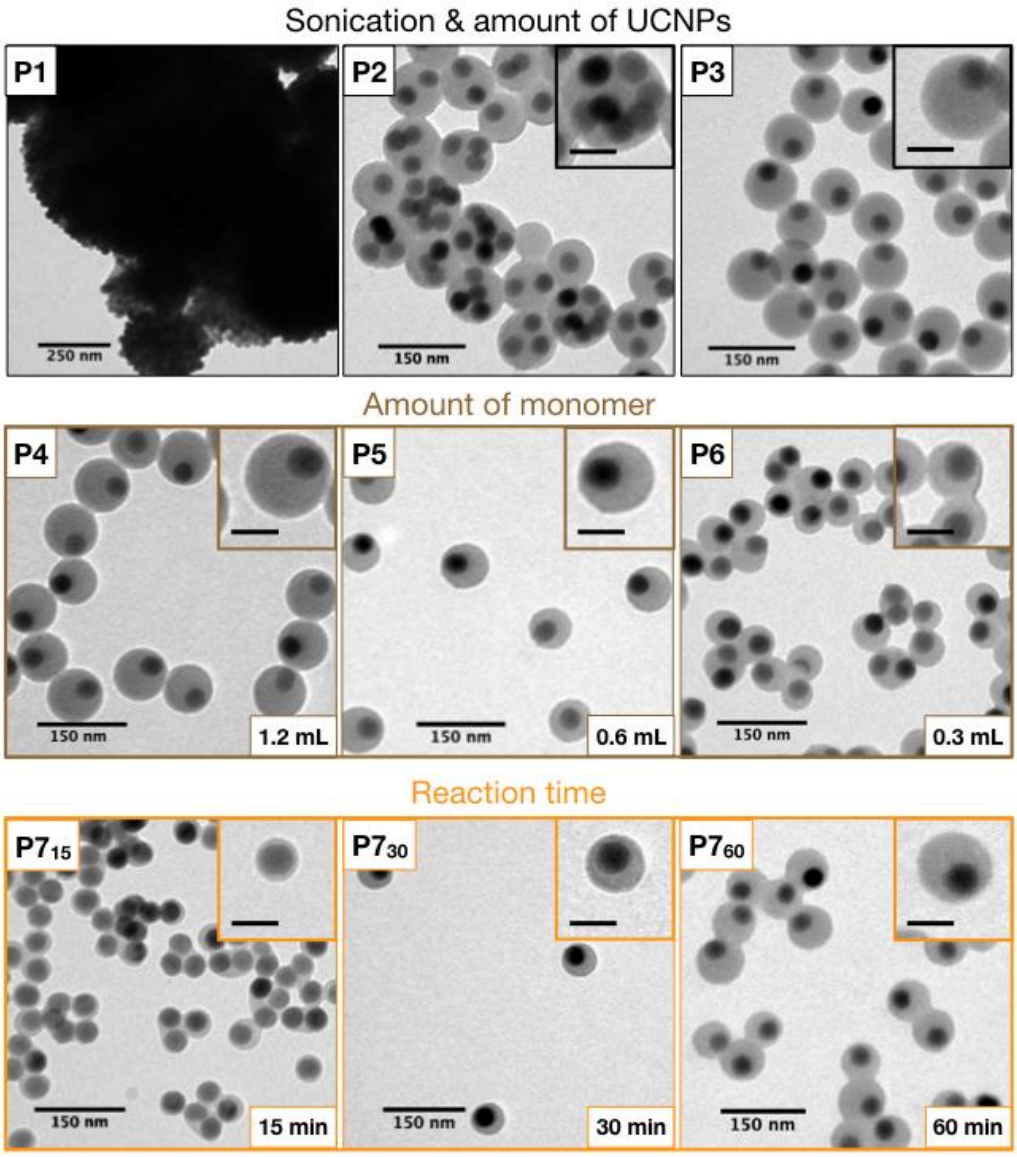

Figure 1. TEM images of: P1) UCNPs@PS aggregates produced when no ultrasonication step is performed; P2) Multi-core@shell UCNPs@PS when incorporating the ultrasonication step into the process. The creation of nanoreactors where polymerization occurs in a confined way is evidenced by the discrete encapsulation of multiple UCNPs; P3) Single-core@shell UCNPs@PS produced after adjusting the initial amount of UCNPs-MDP from 44 mg to 11 mg. P4), P5) and P6) UCNPs@PS produced after adjusting the initial amount of monomer (St) from 1.2 mL to 0.6 mL and 0.3 mL, respectively. $P7_{15}$), $P7_{30}$), and $P7_{60}$) UCNPs@PS produced after quenching the polymerization reaction at 15 min, 30 min, and 60 min after initiation, respectively. All main image scale bars = 150 nm; All inset scale bars = 50 nm

By studying the miniemulsion polymerization process we were able to optimize the coating of the UCNPs-MDP (see Figure 1). Table S1 summarizes the synthetic conditions tested in this

work. First, we confirmed that ultrasonication is essential to form the monomer nanodroplets where the encapsulation of UCNPs-MDP takes place. In the absence of sonication, large submicrometric aggregates of nanoparticles are generated, with poor control of their morphology, as seen in Figure 1-P1. On the contrary, the high energy introduced into the system by using an ultrasonication tip (Scheme 1C-ii) permitted to disrupt and increase the specific surface area of the dispersed phase (i.e., monomer + UCNPs-MDP) in the original emulsion, yielding homogeneous monomer nanodroplets.[47,49] These were effectively stabilized by hexadecane and SDS molecules,[47] allowing the polymerization to proceed within these nanoreactors, and resulting in well-defined nanometric HPSs, see Figure 1-P2. We additionally tested that ultrasonication baths were able to yield similarly excellent results, making this method more easily accessible by commonly available laboratory instrumentation (see Figure S3). The adjustment of the UCNPs-MDP concentration within the dispersed phase, when a fixed amount of SDS and monomer is used, allowed the control of the number of encapsulated UCNPs. Thus, by reducing 4-fold the amount of NPs used during the miniemulsion polymerization, a transition from multi-core shell to single-core shell nanoparticles could be achieved, see Figure 1-P2 and Figure 1-P3, respectively. The partially eccentric location of the core relative to the shell is ascribed to the interfacial tension between the surface of UCNPs-MDP, the monomer/growing polymer shell, and the aqueous phase.[51–54] The resulting UCNPs-MDP coated with PS, or "UCNPs@PS" from now on, were monodisperse in size, featuring 88 ± 4 nm in diameter. In order to reduce light scattering produced by these UCNPs@PS (see dispersion and DLS analyses in Figure S4-Ai, S4-B and S4-D), the PS shell thickness was optimized. As a first strategy, the volume of monomer used for the miniemulsion polymerization was reduced from 1.2 mL to 0.6 mL and to 0.3 mL (Figure 1-P4, P5 and P6, respectively). This allowed us to diminish the mean diameter of the resulting UCNPs@PS from 88 ± 4 nm, to 70 ± 5 nm and to 60 nm ± 5 nm, respectively. Interestingly, when the ratio of SDS/monomer is increased upon reducing the amount of monomer, we observed that the lower volume tested (0.3 mL of St, P6) was accompanied by an increase of multicore UCNPs@PS (23.8%) in comparison with only a ~4.8% of multicore NPs in P5 (0.6 mL of St). This can be explained by the increase in the UCNPs/monomer ratio upon reducing the monomer volume, resulting in an effective increase in the UCNPs concentration. After selecting 0.6 mL as the optimal amount of monomer to be used in our experimental conditions, we tested a kinetic control of the polymerization reaction as an additional way to tune the PS shell thickness (Figure 1-P7_{15} to Figure 1-P7_{60}). The polymerization reaction was stopped by quenching the flask in an ice-bath at 15 min, 30 min, and 60 min after initiation. This method allowed further

control of the size of the UCNPs@PS from 48 ± 5 nm, to 63 ± 4 nm and 70 ± 5 nm (Figure 1-$P7_{15}$, Figure 1-$P7_{30}$ and Figure 1-P_{60}, respectively). Longer reaction times did not substantially increase the final diameter of the UCNP@PS under the tested conditions. The smallest size obtained tended to aggregate, which is ascribed to the incomplete coating of the UCNPs with polystyrene, resulting in hydrophobic regions that led to interparticle interaction and aggregation in aqueous media. Based on the previous experiments we chose the following conditions as optimal in order to obtain single core@shell UCNPs@PS: ultrasonication of the sample, 11 mg of UCNPs-MDP, 0.6 mL of St, and 60 min of polymerization reaction time. These conditions kept a good compromise between coating and protection of UCNPs together with a relatively small size (see dispersion and DLS analyses in Figure S4-Aii, S4-C and S4-E). Finally, modification of the shell composition was explored by varying the monomer concentration added to the reaction from 100 vol% St to 50/50 vol% St/MMA (see Figure 2-P100% to P50%). We observed that upon increasing the vol% of MMA, the resulting polymer shells tended to be thinner. In fact, a final diameter of 58 nm was obtained for P75%, while for P50% we only obtained the same diameter, 58 nm, after increasing 1.5-fold the initial amount of monomer, see Table S1. Further increases in MMA vol% (i.e. St/MMA 25%/75%, synthesis P25%) yielded poorer control over the polymer shell thickness, morphology, and polymerization under our tested conditions (see Figure S5).This can be explained by the increased nucleation and growth of PMMA particles in the aqueous phase, due to the higher polarity of MMA in comparison with St.[55] Still, the incorporation of PMMA to the protective shell was confirmed by FT-IR analyses (see Figure S6), proving the feasibility to easily incorporate different monomers during the polymerization process in order to vary the shell properties of the resulting UCNPs.

2.3. Comparison of protective HPS with a standard poly-acrylic acid (PAA) coating. Given the polar nature of the chemicals responsible for the deterioration of UCNPs upon water-transfer, we reasoned that the most effective way to protect them may be to maintain a robust hydrophobic environment near the UCNPs' surface, avoiding the diffusion of these polar species towards it. This should result in the reduction of all detrimental effects associated with water-transfer of UCNPs, by using one single strategy. In this vein, miniemulsion polymerization has the advantage of isolating UCNPs in hydrophobic nanoreactors (i.e., monomer droplets) until a thick hydrophobic layer of polymer is created, which ensures protection from the aqueous environment, while being negligibly affected by ligand equilibrium due to its solid-like state, contrary to what is expected with other strategies.[30,36] The surface of

the resulting shell is simultaneously decorated with sulfate groups that come from both, chain termination steps with sulfate radicals generated by the initiator (KPS), and SDS surfactant molecules that keep adsorbed after polymerization.[56–58] Sulfate groups deprotonate within a wide range of pHs (pKa < 2), providing colloidal stability in water. The presence of these highly stabilizing surface charges is demonstrated for all HPSs by Z-potential measurements, as seen in Figure 2B. It is noteworthy that the colloidal stability offered by those surface charges is, in principle, higher than that provided to UCNPs by polyacrylic acid (PAA), see Figure 2A & 2B (gray color). PAA is a widely used polydentate ligand for the water-transfer of UCNPs, which provides them with colloidal stability, surface passivation, relative protection in aqueous media, and carboxylic groups that can be used for further bioconjugation.[25,59] For these reasons, we will compare the optical properties and chemical resistance of our HPS-coated UCNPs with more traditional PAA-coated UCNPs used as a control in previous works, from now on "UCNPs-PAA" (see Figure 2A).[33,36,42] The substitution of oleate with MDP as capping agent is accompanied by a decrease in the UCNPs' lifetime of 7% (see Figure 2C), which is ascribed to the change of solvent (from hexane to $CHCl_3$) and to a slight quenching effect produced by the phosphate moiety contained within the MDP structure (see Scheme 1A). The subsequent water-transfer of UCNPs through miniemulsion polymerization results in another reduction in lifetime (8.6%), probably due to the adsorption of a small number of water molecules onto the UCNP's surface. Interestingly, different HPS compositions yielded almost the same exact lifetime (see Figure S7), indicating that the coating process is not substantially affected by changing the hydrophobic monomer, at least within the tested range of compositions.

In contrast, the water-transfer of UCNPs with the traditional PAA ligand results in a pronounced decrease in lifetime (26.2%) when compared with UCNPs-MDP. This is explained by the high permeability of this polydentate ligand to water molecules, which easily reach the UCNPs' surface and produce a strong quenching of their luminescence. The effect of the lifetime reduction on the luminescence properties of these UCNPs was also confirmed by steady-state luminescence measurements, as seen in Figure 2D. In fact, the use of HPSs resulted in UCNPs with about 2-fold more intense upconversion luminescence than the same UCNPs coated with PAA (see Figure S8), which further confirms the effectiveness of our strategy to reduce luminescence quenching in aqueous media.

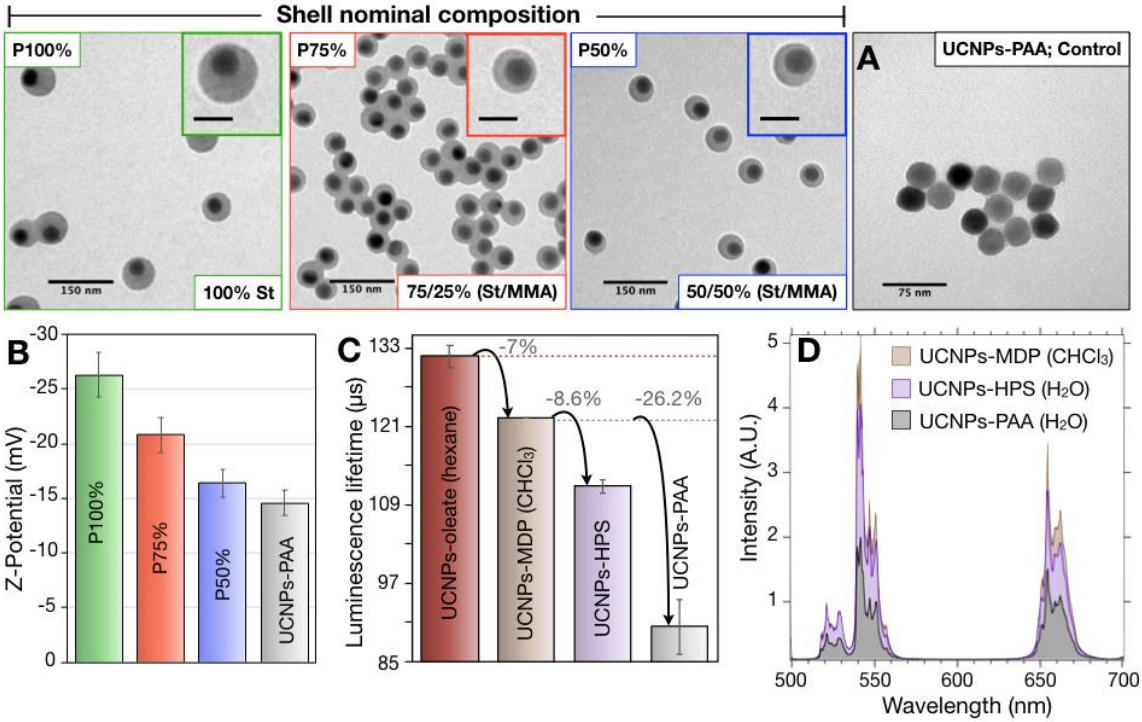

Figure 2. P100%), P75%) and P50%) correspond to TEM images of UCNPs-MDP coated with HPSs with nominal compositions of 100% PS, 75%/25% PS/PMMA, and 50%/50% PS/PMMA, respectively. A) TEM image of UCNPs coated with PAA (control sample). All inset scale bars = 50 nm. B) Z-potential values of P100%, P75%, P50%, and UCNPs-PAA. C) Green emission ($^2H_{11/2} \rightarrow {}^4I_{15/2}$ and $^4S_{3/2} \rightarrow {}^4I_{15/2}$) lifetime values of UCNPs-Oleate (hexane), UCNPs-MDP ($CHCl_3$), UCNPs-HPS (H_2O) and UCNPs-PAA (H_2O). D) Upconversion emission spectra of UCNPs-MDP, UCNPs-HPS and UCNPs-PAA. The protection of UCNPs against water quenching by HPSs is further confirmed, yielding ~2-fold more intense emissions in comparison with UCNPs-PAA. The UCNP core concentration of UCNPs-MDP, UCNPs-HPS and UCNPs-PAA was 100 µg/mL for the lifetime (C) and the steady-state luminescence (D) measurements.

To further assess the protective role of the HPS and compare it with the PAA shell, we carried out long-term stability studies at RT using aqueous dispersions of UCNPs-HPS at very low concentrations (5 µg/mL), which is well below the concentration at which noticeable degradation of UCNPs appear (~50 µg/mL).[15] This low concentration allowed us to study the effect of UCNPs dissolution on their optical and structural/morphological properties (see Figure 3). The degradation of the samples was monitored by following their luminescence intensity for 72 h. Figure 3A shows their luminescence intensity normalized to their initial intensity, as a function of time. Samples P100% and P75% did not exhibit any sign of degradation, since

their luminescence intensity did not change during the 72 h (see green and red lines, respectively). On the other hand, P50% sample (blue line) showed a slight decrease in luminescence intensity of ∽10%, which may be ascribed either to a slightly worse colloidal stability, or a less effective protection compared with P100% and P75%. The luminescence from the UCNPs-PAA sample was highly compromised during the experiment (see black line in Figure 3A). In fact, a strong luminescence decrease took place during the first 3-4 hours, with a reduction of 50% in their luminescence intensity, and after that, a slower decrease continued over time up to 80%. Figure 3B shows the relative luminescence lifetime change of the samples after 72 h, in comparison with the lifetime value yielded by the original non-aged UCNPs samples. These measurements can be used to confirm structural degradation of UCNPs, as reported by other authors.[23,46] Our results confirm once again the degradation of UCNPs-PAA (see Figure 3B, gray bar), as the 72 h aged NPs are accompanied by a ∽11% decrease compared with their original lifetime. Interestingly, the relative lifetime measurements obtained for P100%, P75% and P50% after 72 h (see Figure 3B; green, red and blue bars, respectively) show negligible changes (less than 1%). These results clearly highlight the remarkable protection exhibited by the HPS against UCNPs dissolution. This was also corroborated by TEM, where no damage or structural/morphological changes could be found for the UCNPs-HPS (see Figures 3D, E, and F), whereas the UCNPs-PAA were strongly affected, as shown in Figure 3C. Interestingly, the latter NPs presented a significant reduction of their diameter, from the initial value of 36 nm to a final value of 27 nm. This would mean that the degradation took place at the outer part of the nanoparticle, maintaining the spherical symmetry. After these results, it may seem counterintuitive how the huge relative intensity drops shown by the UCNPs-PAA (∽80%) was accompanied by only a modest relative lifetime decrease (∽11%). However, this can be explained by the fact that UCNPs-PAA's surface is already highly quenched by water, so further lifetime reductions should be mainly due to an increase in UCNPs' surface-to-volume (S/V) ratio as dissolution progresses. On the contrary, the same dissolution process has a more relevant deleterious effect on the UCNPs intensity, as the physical separation and diffusion of Ln^{3+} from the host matrix implies the reduction of the number of sensitizers (Yb^{3+}) and activators (Er^{3+}) that can produce efficient energy transfer, and ultimately photon upconversion. As a direct consequence, the intensity of upconversion luminescence is highly reduced.

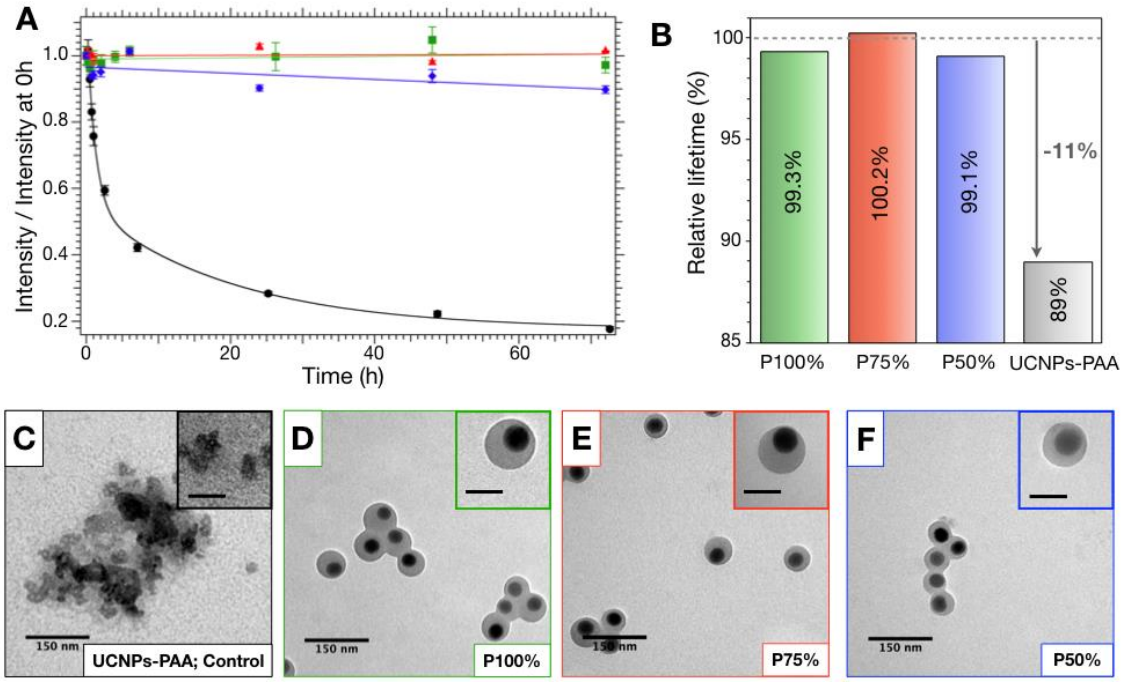

Figure 3. A) Time evolution (0-72 h) of the green upconversion luminescence intensity after dilution of the samples at a core concentration of 5 μg/mL. P100% (green), P75% (red), P50% (blue), UCNPs-PAA (black). B) Relative lifetime change of the green upconversion emission after 72 h, compared with the original lifetime at 0h. P100% (green bar), P75% (red bar), P50% (blue bar), UCNPs-PAA (gray bar). C), D), E) and F) TEM images of UCNPs-PAA, P100%, P75% and P50%, after 72 h in water at a core concentration of 5 μg/mL, respectively. All inset scale bars = 50 nm.

In order to test this hypothesis, we theoretically estimated the reduction of the UCNPs-PAA luminescence intensity by considering the experimentally observed decrease in the UCNP diameter. Two main contributions were taken into account. First, the reduction of the number of ions presents in the UCNP, which is related to the UCNP volume. Second, the decrease of the emission efficiency (quantum yield or lifetime) of the UCNPs-PAA due to surface quenching effects as the nanoparticle S/V ratio increased. These two effects allowed us to properly reproduce the intensity drop of these nanoparticles (see Figure S9). Interestingly, this allowed us to confirm that the main contribution came from the ion dissolution, since more than 50% of ions were estimated to be lost. This result helps to explain why the degradation of the UCNPs showed a smaller decrease in the lifetime than in the luminescence intensity, in agreement with the experimental results. Furthermore, the reduction in UCNP size during dissolution was predicted to follow a logarithmic relationship with time, matching quite accurately the experimental data. We also estimated the solubility product $K_{sp}=[Na^{+}][RE^{3+}][F^{-}]^{4}$,

where RE^{3+} represents the rare-earth ions Y^{3+}, Yb^{3+} and Er^{3+}. For this, we assumed that ions dissolved stoichiometrically. The experimental results (TEM images) showed a mean final diameter below 27 nm which could be related to a RE^{3+} ion dissolution near to 70%. Therefore, the RE^{3+} ion equilibrium concentration was 0.7 times the concentration of RE^{3+} ions in the sample, being 0.0266 mM for a 5 μg/mL of UCNPs. Therefore, the computed solubility product was $K_{sp}=1x10^{-26}$ which roughly agrees with previous values.[15]

We also studied the stability of very diluted samples of UCNPs (5 μg/mL) with different protective shells in potassium phosphate buffer (K^+PB) at a concentration of 100 mM, which is 10 times higher than common phosphate buffer saline (PBS). This buffer quickly and completely degraded the control sample UCNPs-PAA, as can be observed by the 50% luminescence reduction after 1 h and the almost complete disappearance of upconversion luminescence after 72 h (Figure 4A, black line). The reduction in luminescence was such that it was impossible for us to measure the resulting lifetime of the sample (Figure 4B), indicating a profound degradation of the UCNP host matrix and its structure. HR-TEM characterization further confirmed the complete degradation of UCNPs-PAA by K^+PB, yielding a new inorganic phase with an acicular and entangled morphology (see Figure 4C-i). Characterization of the sample by HAADF-TEM indicates the presence of clusters containing atoms of high atomic number (brighter regions), probably traces of aggregated UCNPs-PAA, from which the acicular structures seem to originate. EDX mapping analyses confirm the presence of Phosphorus (P), Ytterbium (Yb), and Yttrium (Y) in these structures (see Figure 5A-i, 5A-ii and 5A-iii, respectively). Noteworthy, the merged image in Figure 5A-iv reveals a spatial correlation between these elements, suggesting that the new phase formed upon UCNPs degradation is composed of a complex mixture of RE phosphates. Most interestingly, we could not detect the presence of fluorine (F) in this sample, suggesting the complete degradation of UCNPs-PAA upon reaction with phosphate and the release of all Fluoride ions (F^-) to the medium in the form of soluble species (e.g., NaF and/or KF). These observations match the results reported in previous works.[23,46] The multiple centrifugations performed prior to HR-TEM characterization, aiming to remove excess K^+PB, may have washed away these water-soluble F^- species, which explains the total absence of Fluorine signal during EDX elemental mapping analyses. More detailed comparative elemental analyses can be found in Figure S10. As opposed to UCNPs-PAA, the long-term luminescence intensity study of P100% and P75% presented a much lower, but still moderate drop in their upconversion luminescence after 72 h (37% and 29% reduction, see Figure 4A green and red symbols, respectively). Nevertheless, when measuring their relative lifetime change, an almost negligible 1.9% and 1.4% decrease was found (Figure 4B

green and red bars, respectively). This suggests that most UCNPs are well protected and preserve their luminescence properties in K^+PB, and that a significant contribution of the luminescence reduction may be attributed to a lower colloidal stability in the buffer, compared to DI-H_2O. In fact, K^+PB forms less soluble potassium SDS salts, and is used in similarly high concentrations in biochemistry protocols to reduce the solubility of SDS, which in our case acts as colloidal stabilizer at the surface of the HPS.[60,61] This could indeed explain the almost negligible change in lifetime, but moderate reduction in luminescence intensity. To further test this hypothesis, we confirmed by DLS that the hydrodynamic diameter (D_H) of P100% and P75% increased in K^+PB compared with the results obtained in DI-H_2O, which can be ascribed to a reduction of the interparticle distance due to a decrease in colloidal stability, see Figure S11. Although this is certainly undesirable, the results from UCNPs-HPS in K^+PB represent a huge improvement in comparison with more traditional coatings, such as UCNPs-PAA. In addition, simply changing SDS by another surfactant that stabilizes the miniemulsion during polymerization may solve this issue. Another possibility would be to modify the polymer shell composition in the future by adding, at late steps of polymerization, an additional monomer containing stabilizing moieties in its structure (e.g., PEG). In order to fully confirm the morphological and structural integrity of P100% and P75%, we performed HR-TEM characterizations of the samples after 72 h aging in K^+PB (see Figure 4D-i and 4D-ii, and Figure 4E-i and 4E-ii, respectively). Figures 4D-i and 4E-i confirmed that the morphology of P100% and P75% has not been affected after 72 h in K^+PB. The quasi-spherical shape of the UCNP cores is conserved, while no sign of the acicular structures formed from the reaction between phosphate and RE^{3+} is detected (see Figure 4C-i and 4C-ii for comparison). A closer look to P100% and P75% (Figure 4D-ii and 4E-ii) further confirmed that no degradation of UCNP cores was present, even at the regions of thinner HPS coating. A higher magnification of these images showing the conserved crystallinity of the NPs can be seen in Figure S12, where the lattice planes can be noticed. As a final chemical and structural characterization, we performed EDX elemental mapping of P100% and P75% (see Figure 5B and 5C, respectively). A strong signal from carbon could be observed in the region corresponding to the HPS, while a void was noticeable at its core, due to the presence of the inorganic UCNP (Figure 5B-i and 5C-i). Within this region, ytterbium, yttrium and fluorine could be identified, matching very nicely the area corresponding to the UCNP core in both samples, see images of Yb, Y and F merged with Carbon in Figures 5B-ii and 5C-ii, 5B-iii (for P100%) and 5C-iii, and 5B-iv and 5C-iv (for P75%), respectively. The high signal obtained from these elements at the UCNP core region is strong evidence that the HPS prevents the leaking of ions from the UCNP towards the solution

and their later reaction with phosphate. In fact, the case of Fluorine is specially revealing, since its high abundance in the core of P100% and P75% suppose a high contrast regarding the total absence of this signal in UCNPs-PAA, where the whole fluoride has been exchanged by phosphate after 72 h in K^+PB (see Figures 5A-i and 5A-iv for comparison). Quite interestingly, we could detect the presence of the MDP ligands at the surface of UCNPs cores, within the HPS, as this is the only possible source of phosphorus that can be present at the UCNP core surface before putting them in contact with K^+PB (see Figure S13). To further verify that MDP was being detected, we also confirmed that phosphorus signal was absent in UCNPs-PAA before ageing in K^+PB (data not shown). The detection of MDP suggests that the growth of the HPS, apart from providing a robust hydrophobic barrier, serves to ensure the long-term passivation of the surface by keeping the phosphate moieties from MDP molecules in place. For further compositional analyses of P100% and P75% after 72 h incubation in K^+PB see Figure S14A & S14B, respectively. Overall, our results indicate that HPS offers great protection against water quenching, ion leaking and dissolution, and chemically harmful species such as phosphate.

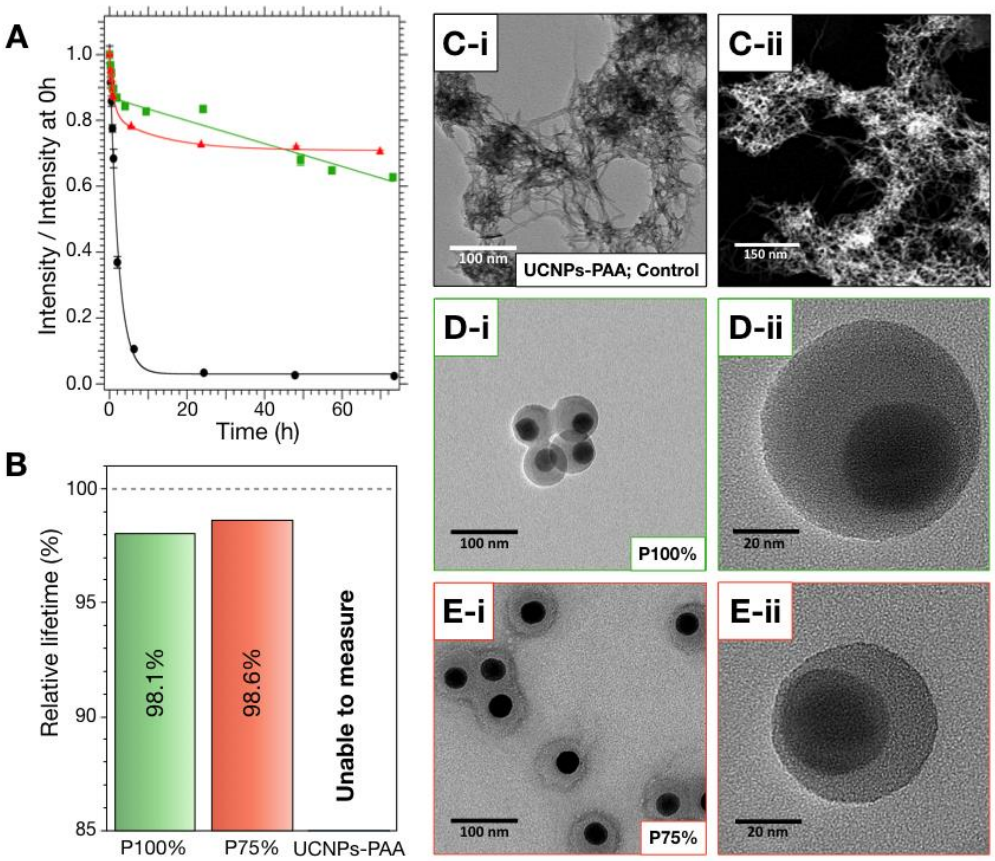

Figure 4. A) Time evolution (0-72 h) of the green upconversion luminescence intensity after dilution of the samples to a core concentration of 5 μg/mL in concentrated K^+PB (100 mM). P100% (green), P75% (red), and UCNPs-PAA (black). B) Relative lifetime change of the green

upconversion emission after 72 h at 5 μg/mL in concentrated K^+PB (100 mM), compared with the original lifetime at 0h. P100% (green bar), P75% (red bar), and UCNPs-PAA (gray bar). HR-TEM images of UCNPs-PAA (C-i; C-ii), P100% (D-i; D-ii) and P75% (E-i; E-ii) after 72 h in K^+PB (100 mM) at a core concentration of 5 μg/mL, respectively. C-ii) HAADF image of UCNPs-PAA, where the brightest regions within the material are likely to contain atoms of higher atomic number.

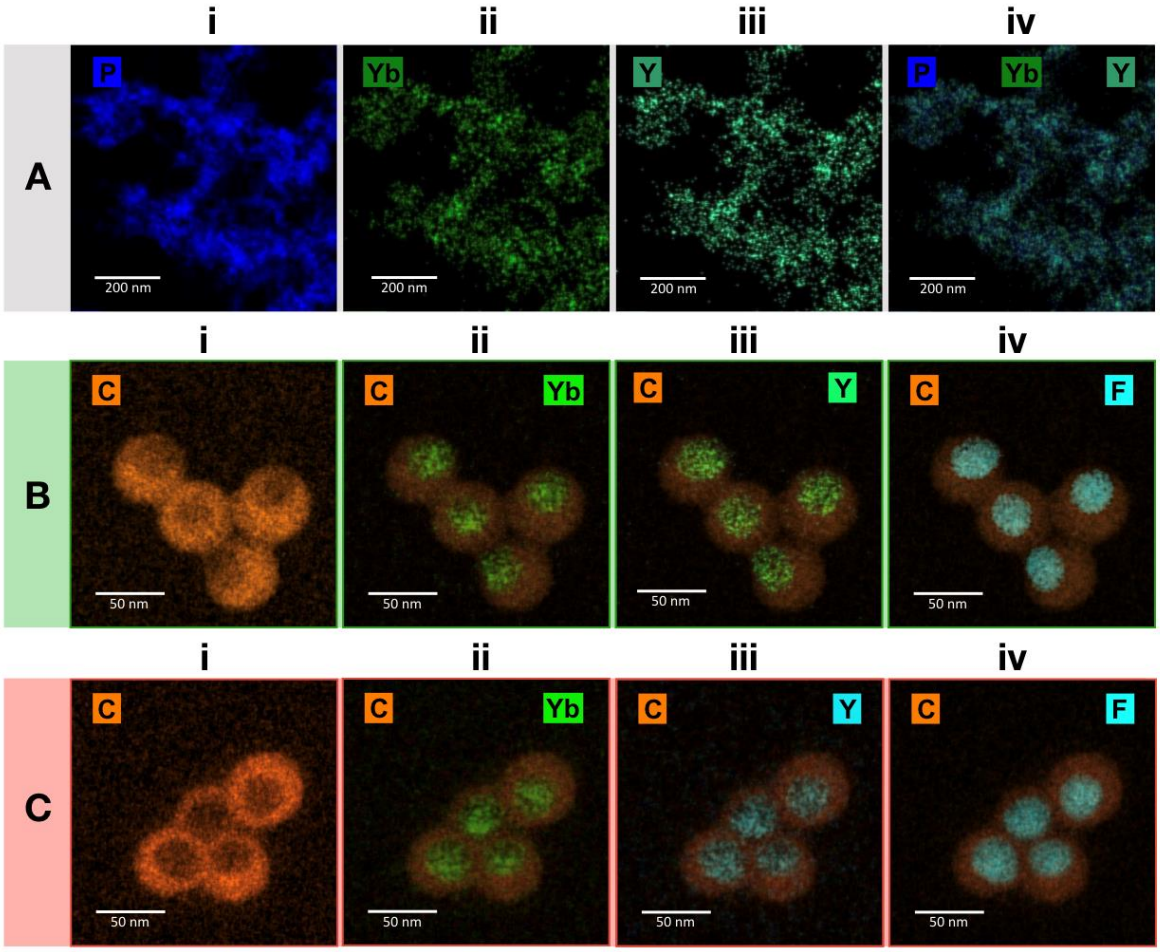

Figure 5. HR-TEM elemental mapping analyses of A) UCNPs-PAA; B) P100%; C) P75%. A-i to A-iv correspond to the signals from elements in UCNPs-PAA: A-i) phosphorous, A-ii) ytterbium, A-iii) yttrium, A-iv) Merged image of phosphorus, ytterbium and yttrium. Scale bar in A-i to A-iv is 200 nm. B-i to B-iv correspond to the elements in P100%: B-i) carbon, B-ii) ytterbium, B-iii) yttrium and B-iv) fluorine. C-i to C-iv correspond to the elements in P75%: C-i) carbon, C-ii) ytterbium, C-iii) yttrium and C-iv) fluorine. Scale bar in B-i to B-iv and in C-i to C-iv is 50 nm.

Aiming to reliably expand the current applications of UCNPs, we explored the potential of HPS as a protecting layer under high-temperature conditions in aqueous media. Thus, we studied the stability of UCNPs in DI-H_2O at 70 ºC and high dilution (5 µg/mL). Again, the HPS offered a much higher protection against degradation than the PAA shell. In fact, UCNPs-PAA are completely degraded in the first 3 h, dropping their luminescence intensity a 90% (see Figure 6A, black). In contrast, P75%, which was selected for yielding the best results in the previous experiments, showed only a 20% reduction (red in Figure 6A). Although this is not a negligible reduction, it is important to highlight that the intensity of P75% after 7 h at 70 ºC is still even higher than that from undegraded (non-aged) UCNPs-PAA at the same concentration. The undetectable luminescence signal obtained for the UCNP-PAA sample after 7 h at 70 ºC made it impossible to determine their lifetime. In contrast, the lifetime remains almost unchanged for P75% (drop ∽3%), see red bar in Figure 6B. This can indicate that the reduction of their luminescence could possibly be ascribed to a very low but non-negligible quenching or degradation of a small fraction of P75%. In this regard, it is reasonable to think that this effect may occur at the regions with the thinnest HPS coating, in the more extremely eccentric UCNPs-HPS. We hypothesize that upon increasing the temperature to 70 ºC, the thinnest shell regions can become partially permeable, allowing some H_2O molecules to reach the UCNPs' surface in a small population of UCNPs-HPS. Still, TEM characterization revealed that, whereas UCNPs-PAA were completely degraded and aggregated due to dissolution/re-precipitation processes (Figure 6C), P75% showed that the HPS effectively protected UCNPs cores even under these extreme conditions (see Figure 6D and Figure S15 for more TEM images). In fact, no sign of particle degradation could be observed by TEM, which may indicate that only a very small fraction of UCNPs-HPS is partially affected. These results are very exciting, considering that they open the possibility to more reliably use UCNPs-HPS in novel applications such as high temperature nanothermometry, nucleic acid amplification techniques such as PCR or isothermal approaches, etc.

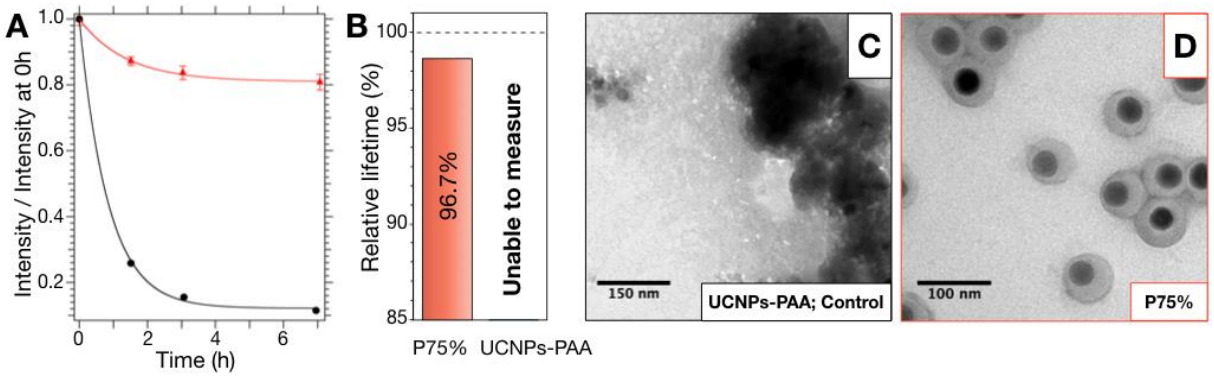

Figure 6. A) Time evolution (0-7 h) of the green upconversion luminescence intensity of the samples with a core concentration of 5 μg/mL in DI-H_2O at 70ºC. P75% (red) and UCNPs-PAA (black). B) Relative lifetime change of the green upconversion emission after 72 h at 5 μg/mL in DI-H_2O at 70 ºC, compared with the original lifetime at 0h. P75% (red bar), UCNPs-PAA (gray bar). C) and D) HR-TEM images of UCNPs-PAA, and P75% after 7 h in DI-H_2O at 70 ºC.

As proven by multiple authors and by our own control experiments with UCNPs-PAA, the transfer of UCNPs to aqueous media by traditional methods is inevitably accompanied by highly detrimental effects. As already mentioned, most proposed strategies aim to avoid degradation by using capping agents or polydentate ligands with high binding affinities, sometimes in a multilayer fashion, to passivate their surface and limit the diffusion of ions.[33,35,42,62,63] Nevertheless, it is important to highlight that these ligands inherently show a hydrophilic character (e.g. PEG-phosphate, poly-phosphates, poly-phosphonates, poly-acrylic acid, poly-sulfonates), necessary to provide UCNPs with the pursued water dispersibility. This implies that they may be usually accompanied by: I) a certain degree of water permeability, and II) unprotected surface regions due to incomplete coating caused by ligand's steric hindrance during functionalization or later detachment.[15,30,36] Thus, although these strategies effectively delay the detrimental effects associated to water-transfer, they can be expected to eventually permit the diffusion of water and other small sized polar molecules towards the surface of the UCNPs, and to the very inner regions of their host matrix as degradation starts, especially in high dilution and non-steady conditions.[15,36] A shocking example of this permeability can be observed in the dissolution of UCNPs coated with silica shells, even when these shells are thick and robust, which can be explained by a certain degree of porosity exhibited by these hydrophilic coatings.[13,15] Only super thick silica shells has recently proved to protect UCNPs at concentrations of 50 μg/mL along a period of 72 h in aqueous media, including phosphates, which represents a significant advance compared with previous attempts, although at the sacrifice of its final size (~ 166 nm in diameter).[25]

Based on our results, the best way to solve these issues is, to our eyes, maintaining a protective hydrophobic environment surrounding the UCNPs, as this will simultaneously cancel all these detrimental mechanisms. In fact, a very recent work by Märkl et al. also points in this direction, by isolating UCNPs with phospholipid bilayers, showing very promising results in different media, including phosphate buffers.[64] In this regard, our strategy has proven to be remarkably effective: all experiments have been performed at very low concentrations (5 μg/mL; similarly

to those used in ultrasensitive bioassays), and, on top of this, under extremely aggressive conditions such as highly concentrated K^+PB (100 mM) and high temperatures (70 ^oC). In-depth characterizations provided strong evidence that HPSs offer a simultaneous solution to all problems associated with water-transfer of UCNPs, namely, water-quenching, dissolution / leaking, and degradation through reaction with chemically aggressive species such as phosphates. Furthermore, the miniemulsion polymerization approach developed herein stands out as a very versatile and affordable approach, which also allows straightforward TEM characterization of the quality and thickness of the resulting HPS coating. Thus, we are convinced that the proven advantages of this strategy, combined with the room for creating exciting new optical and multi-functional systems by embedding additional NPs or moieties within the HPS, will prompt the development of a new wave of lanthanide-doped materials with novel functionalities, as well as with enhanced properties and reliability. A list of nanomaterials that may benefit from our approach is presented in Table S2.

3. Conclusion

In this work we have developed a new methodology to help solve all detrimental effects associated with the transfer of UCNPs to aqueous media. We successfully combined two strategies: i) the substitution of oleate by MDP as capping agent, to achieve higher binding affinity, hydrophobic surface properties and polymerizable groups; and ii) the growth of a robust HPS around the UCNPs to provide long-term and effective protection from the environment. Fine tuning of the number of encapsulated UCNPs, shell thickness, and composition (PS, and PS/PMMA HPS) was demonstrated. Strong evidence of the high protection produced by this HPS against water quenching, dissolution, and degradation by phosphates is shown, even at an atomic level. This was proven under extremely aggressive conditions for UCNPs (high dilution combined with high phosphate concentration or high temperature) and was even more remarkable upon comparison with the very high degradation suffered by UCNPs coated with PAA, used as a control sample. Results from the study on the dissolution of UCNPs-PAA allowed us to theoretically estimate and understand the origins of their luminescence drop. We attributed most of this effect to the release of Ln^{3+} from the host matrix to the environment, while a smaller contribution stems from the loss of quantum efficiency as the S/V ratio of UCNPs increase during dissolution, being this last effect responsible for the lifetime luminescence decrease. This also permitted us to roughly calculate the solubility K_{sp} of β-$NaYF_4$. Finally, we have successfully confirmed the protective role of HPS in aqueous media at 70 ^oC. This lays the foundations to reliably expand the use of UCNPs-

HPS towards applications that involve high temperatures such as PCR, or luminescence nanothermometry. Overall, the proposed strategy stands out as a promising and versatile solution to enhance the properties and reliability, not only of UCNPs, but potentially of other NPs that may experience similar problems upon water-transfer. More interestingly, it offers room for a new generation of multifunctional materials, by taking advantage of the possibilities related to embedding additional moieties within the HPS.

4. Experimental Section

Further details concerning the materials and methods used in this work can be found at the Supporting information "Materials and methods" section.

Synthesis of β-$NaYF_4$: $Yb_{0.20}$,$Er_{0.02}$ (UCNPs): The synthesis of β-$NaYF_4$:$Yb_{0.20}$,$Er_{0.02}$ was carried out by the thermal co-precipitation method in organic media with some modifications.[43] First, $YCl_3 \cdot 6H_2O$ (236.63 mg, 0.78 mmol) $YbCl_3 \cdot 6H_2O$ (77.47 mg, 0.20 mmol) and $ErCl_3 \cdot 6H_2O$ (7.63 mg, 0.02 mmol) were dissolved in 1 mL of MeOH. Then, this solution was added to a 100 mL three-necked round bottom flask, which contained OA (6 mL, 19 mmol) and ODE (15 mL, 46.9 mmol). The resulting flask content was stirred while heated up to 140 ^oC under nitrogen (N_2) flow with a heating rate of 5 ^oC/min. Next, the temperature was maintained for 20 min while the flask was connected to a vacuum pump, in order to remove the traces of water, methanol and hydrochloric acid. After that, the flask was let to naturally cool down to RT. Then, a freshly prepared 10 mL methanol solution containing NaOH (100 mg, 2.5 mmol) and NH_4F (148.16 mg, 4.0 mmol) was added under moderate stirring into the flask containing the dissolved rare earths. The resulting content was mixed for 30 min at 30 ^oC. Then, the mixture was heated up to 110 ^oC (4 ^oC/min) under an N_2 atmosphere and kept for 20 min under vacuum to remove solvent traces. After that, the mixture was heated to 315 ^oC at 16 ^oC/min and kept at this temperature for 1 h. Later, the reaction was allowed to cool down to RT, and the resulting UCNPs were split into four centrifuge tubes. Then, 4 mL of methanol were added to each tube, shaken, and let to separate. The methanol phase was removed, and this process was repeated twice. Next, the product was centrifuged at 7500 Gs for 20 min. Once centrifuged, the supernatant was discarded and the pellets were rinsed, without dispersing them, using 2 mL of ethanol. This process was repeated once. Finally, the pellets were dried at RT for 2 min, dispersed in 4 mL of hexane, and stored for further experiments.

Removal of UCNPs' capping agent: The removal of oleate (capping agent) from the UCNP's surface was performed by a slightly modified method.[65,66] In brief, 8 mL of DMF are added to a 50 mL round bottom flask containing a magnetic stirring bar. Next, 100 mg of UCNPs in hexane are ultrasonicated for 5 min, and carefully added on top of the DMF phase, with no stirring. Then, 100 mg of $NOBF_4$ are added into the flask, and the two phases are mixed for 10 min under vigorous stirring. The removal of oleate from the UCNPs' surface is confirmed by their phase transfer, from hexane to DMF. The DMF phase is then extracted and split into two teflon centrifuge tubes, which are completed by adding $CHCl_3$ and centrifuged at 10000 Gs for 10 min. Next, each pellet is redispersed in 1 mL of DMF and the centrifuge tubes are completed with 7 mL of $CHCl_3$ and centrifuged again. This process is repeated twice more. Finally, the UCNPs are redispersed in 2 mL of DMF and stored.

Surface functionalization of UCNPs with MDP: First, 53 mg of MDP (0.17 mmol) are introduced in a glass vial containing a magnetic stirring bar. Then, 10 mL of $CHCl_3$ are added, and the mixture is stirred vigorously until MDP is completely dissolved. The amount of MDP is always adjusted so that a theoretical surface coating excess corresponding to ~25 MDP molecules per nm^2 of UCNPs is achieved. At this point, 2 mL of uncapped UCNPs (50 mg/mL) in DMF are introduced into the vial, ultrasonicated for 2 min, and let incubate under moderate stirring for 1 h. Then, the resulting UCNPs-MDP dispersion is split into two Teflon centrifuge tubes, 600 μL of hexane are added on top of each one, and they are centrifuged at 13300 Gs for 12 min. Next, the supernatant is carefully discarded, the pellets are redispersed in 7 mL of $CHCl_3$, 600 μL of hexane are added, and the tubes are centrifuged again. This washing process was repeated a total of three times. Finally, the pellets are redispersed in 3 mL of $CHCl_3$ and stored at 4 ^oC in a sealed vial. The concentration of the resulting dispersion, as well as the UCNPs-MDP inorganic/organic weight %, is typically determined by weighting the dry product of a known volume in a precision balance, and by thermogravimetric analysis (TGA). See Thermogravimetric analysis (TGA) in the methods section for further details.

Polymerization of UCNPs-MDP to obtain protective hydrophobic polymer shells (HPSs):
In a typical synthesis, 11 mg of UCNPs-MDP in $CHCl_3$ are centrifuged at 21000 Gs for 10 min. The supernatant is discarded, and the $CHCl_3$ traces are removed from the pellets by using a gentle airflow. The resulting pellet is redispersed in 600 μL of styrene by ultrasonication and centrifuged again. Next, the pellet is redispersed in 600 μL of styrene by ultrasonication (2 min), 7.2 μL of hexadecane are added, and the dispersion is vortexed and ultrasonicated by 2 min.

The dispersion is then added dropwise into a 10 mL round bottom flask containing 4.5 mL of SDS (40 mM) and $NaHCO_3$ (1.2 mM) under vigorous stirring, the flask is capped with a septum, and the mixture is let to homogenize during 1 h. Next, the flask is placed into an ice-bath for 10 min under moderate stirring. After this time, the cooled flask is uncapped, a sonication tip is introduced, and the solution is ultrasonicated for 3 min (Branson 250 Sonifier, analog cell disruptor 200 W max. output power; duty cycle 70%, output power control set at position 1). Once sonicated, the septum-capped flask is stirred for 10 min at RT, after which it is purged with N_2 for 10 min. Then, the flask is immersed in an oil bath (previously heated to 70 ^oC), and the polymerization is started after 4 min by adding 225 µL of potassium persulfate (KPS) initiator (7.5 mg/mL). The mixture is gently stirred at 70 ^oC for 2 h, when the flask is removed from the oil bath and cooled down to RT. The product is split into 5 eppendorf tubes and centrifuged at 21000 Gs for 10 min. The supernatants are discarded, the pellets redispersed in 200 µL of SDS (40 mM), diluted by adding 1 mL of deionized water (DI-H_2O), homogenized by vortexing and centrifuged again. This cleaning process is repeated once again. As a final wash, the pellets are redispersed in 1.2 mL of DI-H_2O, centrifuged again, and redispersed and stored together into a final volume of 1 mL (DI-H_2O).

The synthesis of UCNPs with a HPS composition of 75/25 vol% St/MMA, and with a composition of 50/50 vol% St/ MMA, was performed similarly, but using 450 µL of St + 150 µL of MMA, and 450 µL of St and 450 µL of MMA, respectively. The parameters for all synthesis used in this work can be found in the Supporting Information, Table S1.

Synthesis of UCNPs-PAA (standard surface functionalization; control): Coating of oleate-capped UCNPs with a thin layer of PAA was performed as described elsewhere.[67] 10 mg of UCNPs in hexane are split into two eppendorf tubes and pelleted by centrifugation at 21000 Gs for 10 min. The resulting pellets are then gently dried, in order to remove the traces of hexane. Next, 1 mL of HCl (0.1 M) is added to each eppendorf, and the pellets are redispersed by ultrasonication (5 min). The dispersed UCNPs are then incubated under vigorous shaking at RT for 5 h to remove the oleate molecules acting as capping agent, after which the UCNPs are recovered by centrifugation and the supernatant discarded. Then, the UCNPs are redispersed in 1 mL of DI-H_2O and centrifuged again. After discarding the supernatants, 1 mL of 2.5 wt% PAA aqueous solution (pH=9) is added on top of each UCNP pellet, which is dispersed by ultrasonication and vortexing. The reaction is incubated under vigorous shaking for 16 h at RT, allowing the formation of a thin PAA layer onto the UCNP surface. UCNPs-PAA are recovered by centrifugation (21000 Gs, 10 min). Next, after discarding the supernatants, the nanoparticles

are dispersed in 1 mL of DI-H_2O, and this step is repeated twice. The resulting pellet was finally redispersed in 250 μL of DI-H_2O.

Long-term stability assays at high dilution and RT (DI-H_2O and phosphate buffer): Long-term stability studies of very diluted UCNPs samples (5 μg/mL of UCNPs) were carried out in both DI-H_2O and 100 mM potassium phosphate buffer (K^+PB). We analyzed the aging for the UCNPs with different polymer shells and their results were compared with UCNPs-PAA, used as a control sample. For each sample, as soon as it was diluted to 5 μg/mL and transferred to the cuvette, it was placed inside the temperature controller cell holder (Jasco, ETC-273T), set at 25ºC. After 5 min (considered from here on as time zero), before any significant degradation occurred, we measured the luminescence spectra. Then, we measured the luminescence spectra several times during the next 72 h. For the analysis, all integrated luminescence intensities were normalized to the intensity obtained at time zero. Once the samples aged for 72 h, we also analyzed their decay time at RT and compared it with the decay times obtained for the corresponding not aged samples at a concentration of 100 μg/mL, when chemical degradation is negligible. For TEM characterization after the 72 h stability study in DI-H_2O, samples were concentrated by centrifuging at 21000 Gs during 30 min. In order to prepare the samples for HR-TEM characterization after the 72 h K^+PB stability study, samples were centrifuged 5 times with DI-H_2O in order to remove excess buffer, and finally concentrated in DI-H_2O after the 5th centrifugation step.

Stability assay at high dilution and high temperature (70 ^oC) in DI-H_2O: A long-term stability study of very diluted UCNPs-P75% samples in water at 5 μg/mL was also carried out at high temperature (70 ºC) to analyze the protective role of the HPS in comparison with that provided by the PAA layer. All spectra were taken at 25 ºC to account only for the luminescence decrease due to degradation and not to thermometric properties of the UCNPs luminescence. The protocol was the following: right after diluting the samples at 5 μg/mL, we introduced the cuvette in the temperature controller cell holder at 25 ºC, waited for sample temperature stabilization (5 min), and measured the time zero luminescence spectra. Then, we increased temperature up to 70 ºC, waited for sample temperature stabilization (10 min), and left the samples at 70 ºC for 1 h to permit the disintegration of the UCNPs. After 1 h at 70 ºC, we decreased the temperature again to 25 ºC, waited for sample temperature stabilization (20 min) and then we measured the spectra again. The temperature cycle was repeated six more times until we reached 7 h. Once we finished the experiments, we also analyzed the luminescence

decay time at RT of the samples and compared it with the decay times obtained for the corresponding not aged samples at a concentration of 100 μg/mL, when chemical degradation is negligible.

Acknowledgements

This work has been founded by the Ministerio de Economía y Competitividad-MINECO (MAT2017-83111R), Ministerio de Ciencia, Innovación y Universidades-MICINN (RTI2018-094859-B-100) and by the Comunidad de Madrid (B2017/BMD-3867 RENIM-CM) co-financed by European Structural and Investment Fund. D. M.-G. acknowledges UCM-Santander for a postdoctoral orientation period contract (CT17/17-CT18/17) and the Fundación para la investigación biomédica del Hospital Ramón y Cajal (FIBioHRyC), the Instituto Ramón y Cajal de Investigación Sanitaria (IRyCIS), and the European Commission Horizon 2020 project NanoTBTech (grant number: 801305) for postdoctoral funding. I.Z.G. thanks UCM-Santander for a predoctoral contract (CT63/19-CT64/19). V.T. thanks to Colfuturo and the Colombian government for a predoctoral scholarship. We thank the staff at the ICTS-National Centre for Electron Microscopy (CNME) at the UCM and SCAI (UMA) for the help in the electron microscopy studies.

References

[1] S. Wu, G. Han, D. J. Milliron, S. Aloni, V. Altoe, D. v. Talapin, B. E. Cohen, P. J. Schuck, *Proceedings of the National Academy of Sciences* **2009**, *106*, 10917.

[2] F. Wang, D. Banerjee, Y. Liu, X. Chen, X. Liu, *The Analyst* **2010**, *135*, 1839.

[3] G. Chen, H. Qiu, P. N. Prasad, X. Chen, *Chemical Reviews* **2014**, *114*, 5161.

[4] W. R. Algar, M. Massey, K. Rees, R. Higgins, K. D. Krause, G. H. Darwish, W. J. Peveler, Z. Xiao, H.-Y. Tsai, R. Gupta, K. Lix, M. v. Tran, H. Kim, *Chemical Reviews* **2021**, *121*, 9243.

[5] J. Zhou, Q. Liu, W. Feng, Y. Sun, F. Li, *Chemical Reviews* **2014**, *115*, 395.

[6] D. Mendez-Gonzalez, S. Lahtinen, M. Laurenti, E. López-Cabarcos, J. Rubio-Retama, T. Soukka, *Analytical Chemistry* **2018**, *90*, 13385.

[7] E. Ortiz-Rivero, K. Prorok, M. Skowickł, D. Lu, A. Bednarkiewicz, D. Jaque, P. Haro-González, *Small* **2019**, *15*, 1904154.

[8] F. Vetrone, R. Naccache, A. Zamarrón, A. J. de la Fuente, F. Sanz-Rodríguez, L. M. Maestro, E. M. Rodriguez, D. Jaque, J. G. Solé, J. A. Capobianco, *ACS Nano* **2010**, *4*, 3254.

[9] Y. Xue, C. Ding, Y. Rong, Q. Ma, C. Pan, E. Wu, B. Wu, H. Zeng, *Small* **2017**, *13*, 1701155.

[10] Z. Li, T. Liang, Q. Wang, Z. Liu, *Small* **2020**, *16*, 1905084.

[11] Z. Zhang, Y. Zhang, *Small* **2021**, *17*, 2004552.

[12] M. del Barrio, S. de Marcos, V. Cebolla, J. Heiland, S. Wilhelm, T. Hirsch, J. Galbán, *Biosensors and Bioelectronics* **2014**, *59*, 14.
[13] R. Arppe, I. Hyppänen, N. Perälä, R. Peltomaa, M. Kaiser, C. Würth, S. Christ, U. Resch-Genger, M. Schäferling, T. Soukka, *Nanoscale* **2015**, *7*, 11746.
[14] S. Wilhelm, M. Kaiser, C. Würth, J. Heiland, C. Carrillo-Carrion, V. Muhr, O. S. Wolfbeis, W. J. Parak, U. Resch-Genger, T. Hirsch, *Nanoscale* **2015**, *7*, 1403.
[15] S. Lahtinen, A. Lyytikäinen, H. Päkkilä, E. Hömppi, N. Perälä, M. Lastusaari, T. Soukka, *The Journal of Physical Chemistry C* **2017**, *121*, 656.
[16] O. Dukhno, F. Przybilla, V. Muhr, M. Buchner, T. Hirsch, Y. Mély, *Nanoscale* **2018**, *10*, 15904.
[17] D. Lisjak, O. Plohl, M. Ponikvar-Svet, B. Majaron, *RSC Advances* **2015**, *5*, 27393.
[18] D. J. Gargas, E. M. Chan, A. D. Ostrowski, S. Aloni, M. V. P. Altoe, E. S. Barnard, B. Sanii, J. J. Urban, D. J. Milliron, B. E. Cohen, P. J. Schuck, *Nature Nanotechnology* **2014**, *9*, 300.
[19] I. Halimi, E. M. Rodrigues, S. L. Maurizio, H.-Q. T. Sun, M. Grewal, E. M. Boase, N. Liu, R. Marin, E. Hemmer, *Journal of Materials Chemistry C* **2019**, *7*, 15364.
[20] G. Chen, T. Y. Ohulchanskyy, R. Kumar, H. Ågren, P. N. Prasad, *ACS Nano* **2010**, *4*, 3163.
[21] B. Chen, W. Kong, N. Wang, G. Zhu, F. Wang, *Chemistry of Materials* **2019**, *31*, 4779.
[22] C. Würth, S. Fischer, B. Grauel, A. P. Alivisatos, U. Resch-Genger, *Journal of the American Chemical Society* **2018**, *140*, 4922.
[23] O. Plohl, M. Kraft, J. Kovac, B. Belec, M. Ponikvar-Svet, C. Würth, D. Lisjak, U. Resch-Genger, *Langmuir* **2017**, *33*, 553.
[24] G. Zhao, L. Tong, P. Cao, M. Nitz, M. A. Winnik, *Langmuir* **2014**, *30*, 6980.
[25] M. I. Saleh, B. Rühle, S. Wang, J. Radnik, Y. You, U. Resch-Genger, *Scientific Reports* **2020**, *10*, 19318.
[26] Y. C. Chang, M. Y. Chou, *Oral Surgery, Oral Medicine, Oral Pathology, Oral Radiology, and Endodontology* **2001**, *91*, 230.
[27] A. Verma, D. Ali, A. K. Pathak, *Toxicological & Environmental Chemistry* **2017**, *99*, 148.
[28] P. M. A. Salomão, F. A. de Oliveira, P. D. Rodrigues, L. P. Al-Ahj, K. C. da S. Gasque, P. Jeggle, M. A. R. Buzalaf, R. C. de Oliveira, J. M. Edwardson, A. C. Magalhães, *PLOS ONE* **2017**, *12*, e0179471.
[29] S. Hirano, K. T. Suzuki, *Environmental Health Perspectives* **1996**, *104*, 85.
[30] R. Li, Z. Ji, J. Dong, C. H. Chang, X. Wang, B. Sun, M. Wang, Y.-P. Liao, J. I. Zink, A. E. Nel, T. Xia, *ACS Nano* **2015**, *9*, 3293.
[31] S. von Euw, Y. Wang, G. Laurent, C. Drouet, F. Babonneau, N. Nassif, T. Azaïs, *Scientific Reports 2019 9:1* **2019**, *9*, 1.
[32] E. Palo, M. Salomäki, M. Lastusaari, *Journal of Colloid and Interface Science* **2019**, *538*, 320.
[33] E. Palo, S. Lahtinen, H. Päkkilä, M. Salomäki, T. Soukka, M. Lastusaari, *Langmuir* **2018**, *34*, 7759.
[34] Q. Zhang, K. Song, J. Zhao, X. Kong, Y. Sun, X. Liu, Y. Zhang, Q. Zeng, H. Zhang, *Journal of Colloid and Interface Science* **2009**, *336*, 171.

[35] J.-C. Boyer, M.-P. Manseau, J. I. Murray, F. C. J. M. van Veggel, *Langmuir* **2009**, *26*, 1157.
[36] S. F. Himmelstoß, T. Hirsch, *Particle & Particle Systems Characterization* **2019**, *36*, 1900235.
[37] U. Kostiv, V. Lobaz, J. Kučka, P. Švec, O. Sedláček, M. Hrubý, O. Janoušková, P. Francová, V. Kolářová, L. Šefc, D. Horák, *Nanoscale* **2017**, *9*, 16680.
[38] P. Cao, L. Tong, Y. Hou, G. Zhao, G. Guerin, M. A. Winnik, M. Nitz, *Langmuir* **2012**, *28*, 12861.
[39] G. Jiang, J. Pichaandi, N. J. J. Johnson, R. D. Burke, F. C. J. M. van Veggel, *Langmuir* **2012**, *28*, 3239.
[40] M. Liras, M. González-Béjar, E. Peinado, L. Francés-Soriano, J. Pérez-Prieto, I. Quijada-Garrido, O. García, *Chemistry of Materials* **2014**, *26*, 4014.
[41] W. Zhang, B. Peng, F. Tian, W. Qin, X. Qian, *Analytical Chemistry* **2014**, *86*, 482.
[42] N. Estebanez, M. González-Béjar, J. Pérez-Prieto, *ACS Omega* **2019**, *4*, 3012.
[43] Z. Li, Y. Zhang, *Nanotechnology* **2008**, *19*, 345606.
[44] H. Chen, Y. Lang, D. Zhao, C. He, W. Qin, *Journal of Fluorine Chemistry* **2015**, *174*, 70.
[45] P. R. Griffiths, *Vibrational Spectroscopy* **1992**, *4*, 121.
[46] E. Andresen, C. Würth, C. Prinz, M. Michaelis, U. Resch-Genger, *Nanoscale* **2020**, *12*, 12589.
[47] J. M. Asua, *Progress in Polymer Science* **2002**, *27*, 1283.
[48] S. W. Zhang, S. X. Zhou, Y. M. Weng, L. M. Wu, *Langmuir* **2005**, *21*, 2124.
[49] K. Landfester, in *Top Curr Chem*, Springer, Berlin, Heidelberg, **2003**, pp. 75–123.
[50] G. Jia, Y. Xu, X. Tan, N. Cai, *Iranian Polymer Journal (English Edition)* **2006**, *15*, 979.
[51] S. Xu, W.-F. Ma, L.-J. You, J.-M. Li, J. Guo, J. J. Hu, C.-C. Wang, *Langmuir* **2012**, *28*, 3271.
[52] J. Ge, Y. Hu, T. Zhang, Y. Yin, *Journal of the American Chemical Society* **2007**, *129*, 8974.
[53] C. Hübner, C. Fettkenhauer, K. Voges, D. C. Lupascu, *Langmuir* **2018**, *34*, 376.
[54] Y. Li, B. Liu, *ACS Macro Letters* **2017**, *6*, 1315.
[55] C. S. Chern, C. H. Lin, *Polymer* **2000**, *41*, 4473.
[56] M. Lundqvist, J. Stigler, G. Elia, I. Lynch, T. Cedervall, K. A. Dawson, *Proceedings of the National Academy of Sciences of the United States of America* **2008**, *105*, 14265.
[57] J. A. Bonham, F. Waggett, M. A. Faers, J. S. van Duijneveldt, *Colloid and Polymer Science* **2017**, *295*, 479.
[58] J. Sefcik, M. Verduyn, G. Storti, M. Morbidelli, *Langmuir* **2003**, *19*, 4778.
[59] A. Sedlmeier, H. H. Gorris, *Chemical Society Reviews* **2015**, *Advance*, DOI: 10.1039/C4CS00186A.
[60] R. E. Farrell, in *RNA Methodologies*, Academic Press, **2005**, pp. 47–66.
[61] Z. Zaman, R. L. Verwilghen, *Analytical Biochemistry* **1979**, *100*, 64.
[62] M. Vozlič, T. Černič, S. Gyergyek, B. Majaron, M. Ponikvar-Svet, U. Kostiv, D. Horák, D. Lisjak, *Dalton Transactions* **2021**, *50*, 6588.
[63] R. Naccache, F. Vetrone, V. Mahalingam, L. A. Cuccia, J. A. Capobianco, *Chem. Mater.* **2009**, *21*, 717.

[64] S. Märkl, A. Schroter, T. Hirsch, *Nano Letters* **2020**, *20*, 8620.
[65] A. Dong, X. Ye, J. Chen, Y. Kang, T. Gordon, J. M. Kikkawa, C. B. Murray, *J. Am. Chem. Soc* **2011**, *133*, 998.
[66] V. Muhr, C. Würth, M. Kraft, M. Buchner, A. J. Baeumner, U. Resch-Genger, T. Hirsch, *Analytical Chemistry* **2017**, *89*, 4868.
[67] N. Sirkka, A. Lyytikäinen, T. Savukoski, T. Soukka, *Analytica Chimica Acta* **2016**, *925*, 82.

The stunning optical properties of upconverting nanoparticles (UCNPs) face highly detrimental effects when transferred to aqueous media for bio-applications. In this work, the origin and extent of these effects are studied, while a coating strategy is rationally developed and optimized to effectively overcome these drawbacks. The results indicate that UCNPs with reliable properties and expanded biomedical applications are possible.

Diego Mendez-Gonzalez,* Vivian Torres Vera, Irene Zabala Gutierrez, Concepción Cascales, Jorge Rubio-Retama, Oscar G. Calderón, Sonia Melle,* Marco Laurenti.*

Upconverting nanoparticles in aqueous media: not a dead-end road. Avoiding degradation by using hydrophobic polymer shells.

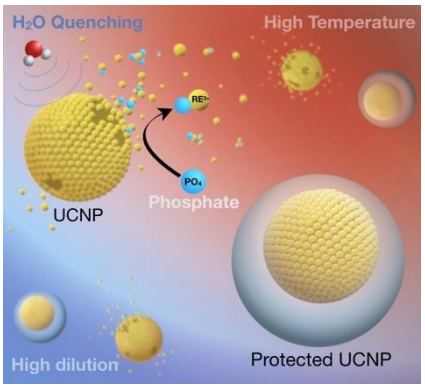

Supporting Information

Upconverting nanoparticles in aqueous media: not a dead-end road. Avoiding degradation by using hydrophobic polymer shells.

Diego Mendez-Gonzalez, Vivian Torres Vera, Irene Zabala Gutierrez, Concepción Cascales, Jorge Rubio-Retama, Oscar G. Calderón, Sonia Melle,* Marco Laurenti.**

This supporting information includes the following sections:

I) Materials and methods

1. Materials

Yttrium (III) chloride hexahydrate ($YCl_3 \cdot 6H_2O$, 99.99%), ytterbium (III) chloride hexahydrate ($YbCl_3 \cdot 6H_2O$, 99.9%), erbium (III) chloride hexahydrate ($ErCl_3 \cdot 6H_2O$, 99.9%), 1-octadecene (ODE, 80%), oleic acid (OA, 90%), sodium hydroxide (98%), ammonium fluoride (98%), n-hexane (95%), methanol (99.9%), dimethyl sulfoxide (DMSO, ≥ 99.9%), chloroform ($CHCl_3$, ≥ 99.8%), N,N-dimethylformamide (DMF, > 99%), Nitrosyl tetrafluoroborate (NOBF, 95%), styrene (>99%), methyl methacrylate (99%), hexadecane (HD, 99%), sodium dodecyl sulfate (SDS, > 99%), sodium bicarbonate ($NaHCO_3$, 99.5%), potassium persulfate (KPS, ≥ 99.9%), Poly-acrylic acid (PAA; Concentration = 50 wt% in water; Mw ~ 2000 g/mol) and potassium phosphate dibasic trihydrate (≥99%, Reagent Plus) were purchased from Sigma-Aldrich (Merck). 10-methacryloyldecylphosphate (MDP, 99%) was purchased from LGC Group, Spain.

2. Methods

a) Ultrasonication

The ultrasonication step for the miniemulsion formation was performed by using an ultrasonication tip (Branson 250 Sonifier, analog cell disruptor; 200 W max. output power) working at a duty cycle of 70% and the output power set at position “1” (which adjusts amplitude of power supply output voltage to 10% nominal converter amplitude). The viability of replacing this equipment with a more traditional ultrasonication bath (JP Selecta, Ultrasons

Series; 50W, 0.5L volume capacity) was eventually tested (see synthesis P8 in Table S1 and Figure S3 in Supporting Information).

b) Transmission electron microscopy (TEM) characterization

TEM images were acquired by using a JEOL JEM 1010 working at 80 kV and a GATAN Megaview II digital camera. High resolution TEM (HR-TEM) images were obtained using a JEOL JEM 2100 working at 200 kV and coupled to a GATAN Orius SC1000 digital camera. Samples were prepared by depositing a drop of UCNPs dispersion onto Formvar-coated copper grids and dried at RT. High-angle annular dark-field (HAADF) scanning TEM (STEM) and energy-dispersive X-ray (EDX) mappings were conducted by using a FEI Talos F200X (ThermoFisher Scientific, USA) coupled to an EDX detector.

c) Fourier transform Infrared (FT-IR) spectroscopy

A Thermo Nicolet 200IR spectrometer was used to obtain FT-IR spectra. Samples were prepared by grinding the dried nanoparticles with potassium bromide (KBr) until a thin powder was obtained. Then, the powder was transformed into a pellet by using a mechanical press (working at 10-ton) while air and moisture were removed using a vacuum pump. Background and sample spectra were acquired working in absorbance mode with a resolution of 4 cm^{-1} and 128 scans. Spectra were H_2O and CO_2 corrected.

d) Thermogravimetric analysis (TGA)

TGA analyses were performed using a TGA/DSC 1 STAR system (Mettler Toledo). In a typical experiment, concentrated samples (~6 mg of nanoparticles) were deposited and dried at 82 ºC in a 70 μL alumina crucible, which was weighed before and after sample addition and drying by using both the TGA/DSC internal microbalance and an external microbalance (AT261 DeltaRange, Mettler Toledo), for comparison. The samples were then introduced into the TGA/DSC and after stabilization, the experiment was started. The heating program consisted in i) heating to 120 ºC at a heating rate of 5 ºC/min; ii) holding the temperature at 120 ºC for 30 min to evaporate traces of adsorbed water; iii) increasing the temperature to 530 ºC at a rate of 10 ºC/min; iv) maintaining the temperature at 530 ºC for 10 min; v) returning to the starting temperature. The gas flows used during the experiments were 20 cm^3/min for O_2 and N_2, respectively. The inorganic/organic weight % of UCNPs-MDP is typically 95% core/5% capping agent, while the studied UCNPs-HPS typically oscillates between 48% core/ 52% shell and 56% core/44% shell.

e) Z-Potential

Z-potential measurements were carried out with a Malvern Nano-ZS instrument. The samples for Z-potential experiments were freshly prepared before measurements, by diluting them to a final concentration of ~50 μg/mL. The measurements were acquired at 25 ^{o}C using the automatic mode (10 minimum runs – 100 maximum runs), with an equilibration time of 120 seconds and the Smoluchowski fit model. A minimum of 3 independent measurements were performed for each sample.

f) Steady-state photoluminescence measurements

A home-built system was used to acquire the UCNPs photoluminescent emission spectra. The 976 nm excitation laser beam is generated by a pigtailed 10 W CW laser (JDSU, L4-9897603), which also contains a current and temperature controller (ILX Lightwave; LDX-36025-12 and LDT-5525B, respectively). The laser beam first goes through a long-pass dichroic filter (Semrock, FF757-Di01), and it is then focused on a 3 mm path length cuvette placed inside a temperature chamber cell (Jasco, ETC-273T). The excitation irradiance in the sample was 0.1 kW/cm^2 much lower than the saturation intensity of the $^2F_{7/2} \rightarrow {}^2F_{5/2}$ transition of Yb^{3+} ions. The upconversion photoluminescence coming from the sample is reflected by the dichroic mirror towards two short-pass filters (Semrock, FF01-775/SP and Thorlabs, FESH0750) that block the scattered infrared radiation from the laser at 976 nm. Then, the upconversion photoluminescence coming from the sample is focused into an optical fiber that is connected to a monochromator (Horiba Jobin Yvon, iHR320). This monochromator is equipped with a photomultiplier tube (Hamamatsu, R928) and uses an 1800 g/mm grating. Photoluminescence spectra of the different UCNPs were obtained by taking three consecutive spectra. Then, the average intensity of the integrated area within the spectra from the studied emission bands were computed, taking the maximum deviation as the average error. The results that are presented without error bars correspond to a single representative measurement.

g) Photoluminescence lifetime measurements

The time-resolved photon counting method was used to determine the luminescence lifetime of the different samples. Excitation pulses of duration 40 μs (with 125 Hz repetition rate) were generated with the laser current controller (LDX-36025-12, from ILX Lightwave). Luminescence emissions were detected by the photomultiplier tube directly connected (without using a pre-amplifier step) to a 50 Ω input of a digital oscilloscope (Agilent, DSO9104A). The

oscilloscope is triggered by using a signal from the laser current controller. Our own developed Matlab program was used to analyze in real-time each recorded signal, directly in the oscilloscope. This code simulates the discriminator and the multichannel counter. After analyzing more than 5000 trigger signals, a luminescence decay curve was obtained. The luminescence lifetime was obtained by fitting the decay curves to a double exponential function. Fitting was done from the time where the luminescence reached 60% of its maximum value to the final recorded time (2 ms, long enough to ensure the complete decay of luminescence). We made use of the short decay time to compare lifetime decays for samples with different coatings since this time is usually related to surface quenching effects. For the long-term stability analysis (whose results are displayed in Figures. 3, 4 and 6) all samples were diluted to 5 μg/mL. Thus, we needed to increase the excitation pulse duration to 500 μs (with 50 Hz repetition rate) to achieve detectable luminescence signals after 72 h for the less protected UCNPs coated with PAA.

h) Dynamic light scattering (DLS)

The hydrodynamic diameter (D_h) of the samples was obtained using a ZetaSizer Nano ZS (Malvern Instruments). Accumulation time was automatically determined for each sample. The multimodal analysis method was selected within the DLS software provided by Malvern. The z-average was calculated from the correlation function, and the D_h was derived using the Einstein-Stokes equation. For the DLS experiments, the samples were diluted to ~50 μg/mL.

II) Results

0. Summary of tested miniemulsion polymerization conditions.

Table S1. List of different conditions tested during miniemulsion polymerization.

Sample name	UCNPs (mass)	Composition (%vol)	Monomer (vol)	Reaction time	Ultrasonication
P1	44 mg	St (100%)	1.2 mL	60 min	No
P2	44 mg	St (100%)	1.2 mL	60 min	Yes (tip)
P3	11 mg	St (100%)	1.2 mL	60 min	Yes (tip)
P4	11 mg	St (100%)	1.2 mL	60 min	Yes (tip)
P5	11 mg	St (100%)	0.6 mL	60 min	Yes (tip)
P6	11 mg	St (100%)	0.3 mL	60 min	Yes (tip)
$P7_{15}$	11 mg	St (100%)	0.6 mL	15 min	Yes (tip)
$P7_{30}$	11 mg	St (100%)	0.6 mL	30 min	Yes (tip)
$P7_{60}$	11 mg	St (100%)	0.6 mL	60 min	Yes (tip)
P100%	11 mg	St (100%)	0.6 mL	60 min	Yes (tip)
P75%	11 mg	St / MMA (75/25%)	0.45 mL / 0.15 mL	60 min	Yes (tip)
P50%	11 mg	St / MMA (50/50%)	0.45 mL / 0.45 mL	60 min	Yes (tip)
P25%	11 mg	St / MMA (25/75%)	0.15 mL / 0.45 mL	60 min	Yes (tip)
P8	11 mg	St / MMA (50/50%)	0.45 mL / 0.45 mL	60 min	Yes (bath)

During these experiments the aqueous phase (4.5 mL; SDS 40 mM; $NaHCO_3$ 1.2 mM), hexadecane (24.6 µmoles), initiator (KPS; 225 µL, 7.5 mg / mL) and polymerization temperature (70°C) were kept constant.

1. TEM, HR-TEM and SAED images of ß-$NaYF_4$:$Yb_{0.20}$,$Er_{0.02}$ (UCNPs).

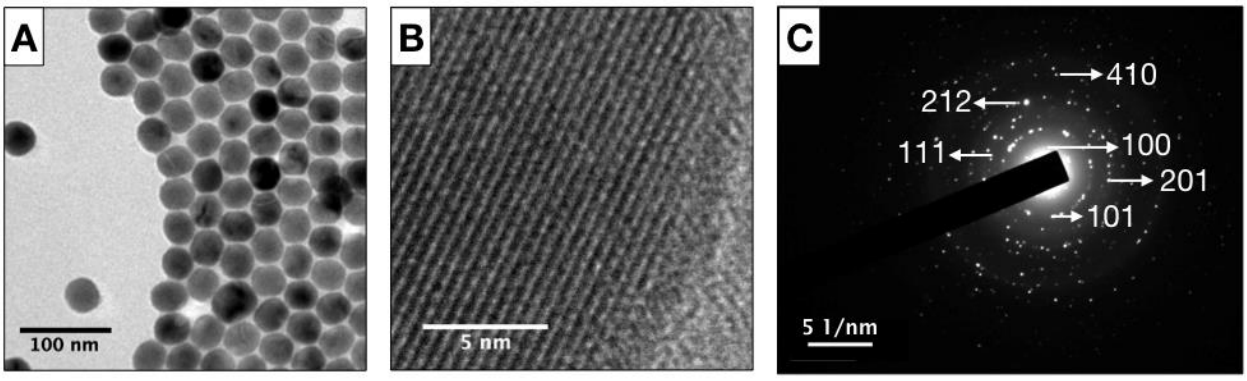

Figure S1. A) TEM image of oleate-capped UCNPs, showing their monodisperse, quasi-spherical morphology. B) HR-TEM magnification of an oleate-capped UCNP, showing the 100-lattice plane from $NaYF_4$ hexagonal phase. C) Selected Area Electron Diffraction (SAED) pattern from oleate-capped UCNPs. Planes 100 (d = 0.515 nm), 101 (d = 0.290 nm), 111 (d = 0.227 nm), 201 (d = 0.207 nm), 212 (d = 0.130 nm) and 410 (d = 0.112 nm) from $NaYF_4$ hexagonal phase are easily identified, confirming that $NaYF_4$ is in its hexagonal phase according to the JCPDS 16-0334 diffraction card.

2. TEM images comparing Snowman-like UCNPs@PS and core@shell UCNPs@PS.

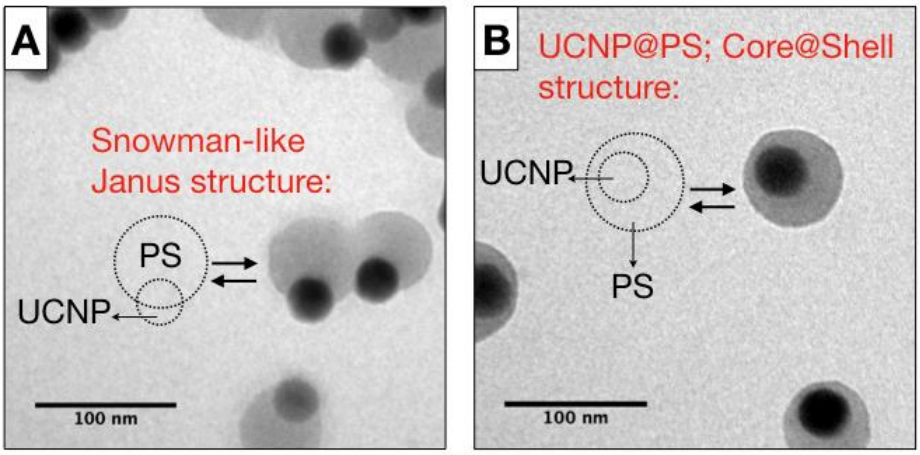

Figure S2. A) TEM image of UCNPs-oleate coated with polystyrene shells. The reduced wetting between the oleate capped UCNPs and the polystyrene shell results in NP / Shell phase separation, yielding Snowman-like Janus structures where the UCNPs are exposed to the environment. B) TEM image of UCNPs-MDP coated with polystyrene shells. The improved wetting allows the formation of core@shell structures, were the UCNPs (cores) are protected from the environment.

3. TEM images of UCNPs@PS/PMMA (50%/50%) resulting from using an ultrasonication bath.

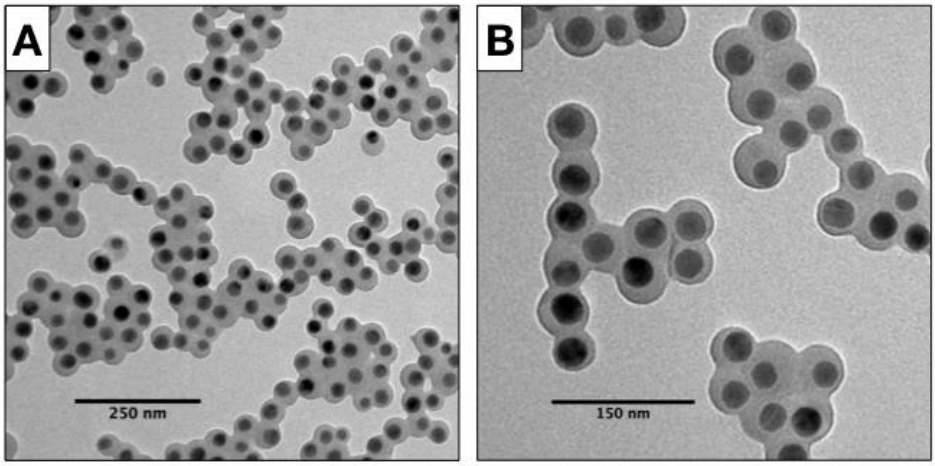

Figure S3. A) TEM image of synthesis P8 (50%/50% St/MMA). B) TEM image magnification of synthesis P8. This synthesis was performed by using an ultrasonication bath, instead of an ultrasonication tip, demonstrating the viability of using commonly available laboratory

instrumentation (ultrasonic baths) to produce high quality UCNPs coated with protective polymer shells, featuring single core@shell morphologies.

4. Photographs depicting different light scattering and DLS analyses of UCNPs@PS with different sizes.

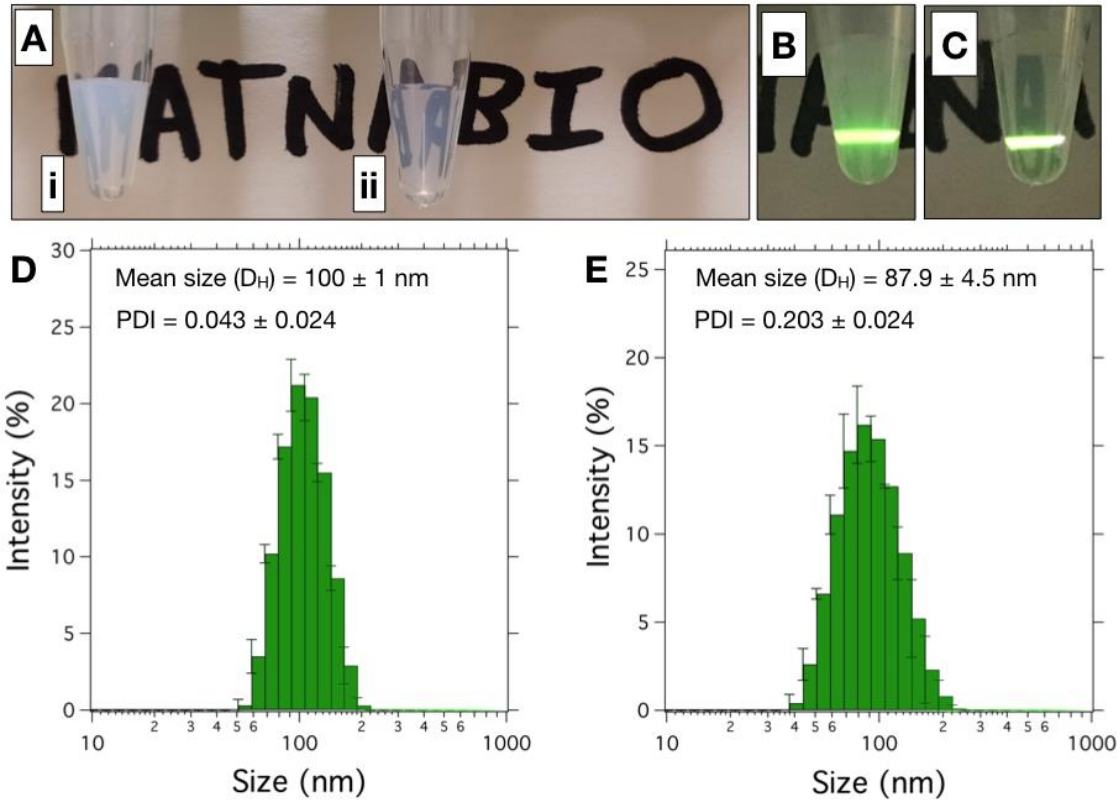

Figure S4. A) Photograph of 1 mg/mL dispersions of UCNPS@PS for particles with different TEM diameters: i) ⦰ = 88 nm and ii) ⦰ = 70 nm. B & C) Emission from the dispersion shown in A.i) & A.ii), respectively, both under CW excitation with a 980 nm laser (∽250 W/cm^2). The reduction on light scattering is evident upon reducing the nanoparticle diameter, resulting in clearer dispersions (Fig. S4A.ii) and sharper emissions (Fig. S4C). D) & E) DLS Intensity size distributions of the previous UCNPs@PS. These analyses yielded a mean hydrodynamic diameter (D_H) = 100 ± 1 nm and D_H = 87.9 ± 4.5 nm for the UCNPs@PS with TEM ⦰ = 88 nm and ⦰ = 70 nm, respectively.

5. TEM image of UCNPs@PS/PMMA (25%/75%).

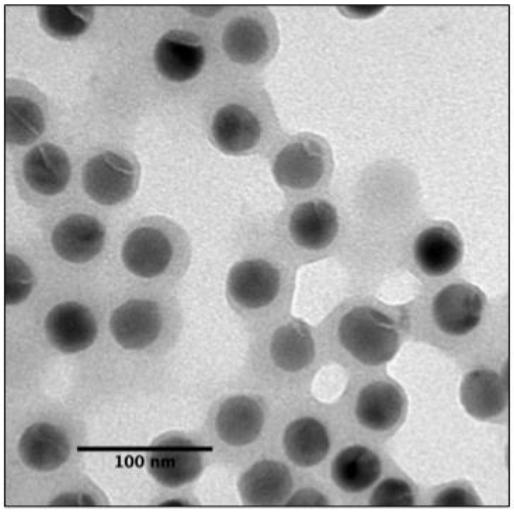

Figure S5. UCNPs coated with a HPS containing 25%/75% St/MMA nominal composition (synthesis P25%). As observed by the TEM image, the increase of MMA beyond 50% yielded thinner shells, and poorer control on the polymerization process and the overall HPS homogeneity.

6. FT-IR Analyses of UCNPs@PS and UCNPs@PS/PMMA (50%/50%).

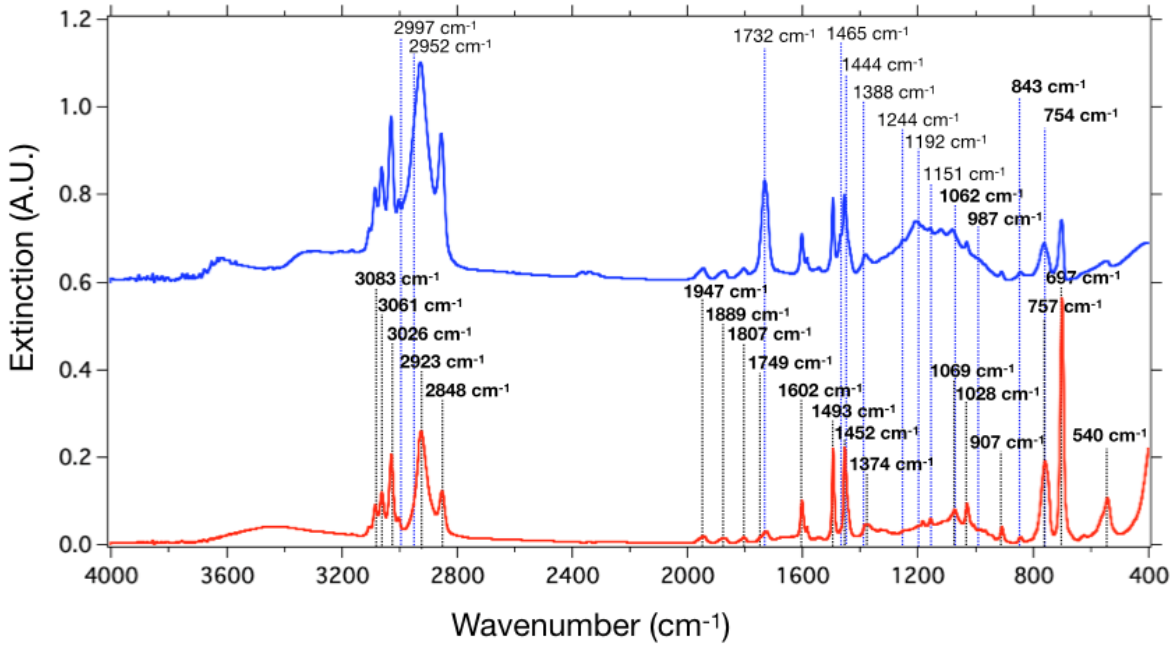

Figure S6. FT-IR spectra of UCNPs@PS, red line; and UCNPs@PS/PMMA (50%/50% St/MMA), blue line. The identification of the main characteristic peaks has been summarized next, according to data reported elsewhere:[1-3]

Characteristic PS and common PS/PMMA peaks

PS	Band assignment
3083 cm^{-1}	ν_{20B} (B_1)
3061 cm^{-1}	$\nu_{20A'}$ (A_1)
3026 cm^{-1}	$\nu_{2'}$ (A_1)
2923 cm^{-1}	-CH_2 asymmetric stretching
2848 cm^{-1}	-CH_2 symmetric stretching
1947 cm^{-1}	Aromatic combination bands in mono-substituted rings
1889 cm^{-1}	
1807 cm^{-1}	
1749 cm^{-1}	
1602 cm^{-1}	ν_{9B} (B_1)
1493 cm^{-1}	ν_{19} (A_1)
1452 cm^{-1}	δ (CH_2); ν_{19B} (B_1)
1374 cm^{-1}	ν_{14B} (B_1)
1069 cm^{-1}	$\nu_{18B'}$ (B_1)
1028 cm^{-1}	ν_{18A} (A_1)
907 cm^{-1}	ν_{17} (B_2)
757 cm^{-1}	ν_{10B} (B_2)
697 cm^{-1}	ν_{11} (B_2)
540 cm^{-1}	ν_4 (B_2)

Characteristic PMMA peaks

PMMA	Band assignment
2997 cm^{-1}	(O)CH_3 stretching
2952 cm^{-1}	(O)CH_3 stretching
1732 cm^{-1}	C=O stretching
1465 cm^{-1}	(O)CH_3 bending
1250 cm^{-1} to 1150 cm^{-1}	Vibrations from ester groups of PMMA
987 cm^{-1}	(O)CH_3 rocking coupled with C-O-C stretching

7. Lifetime decay curves of P100%, P75% and P50%.

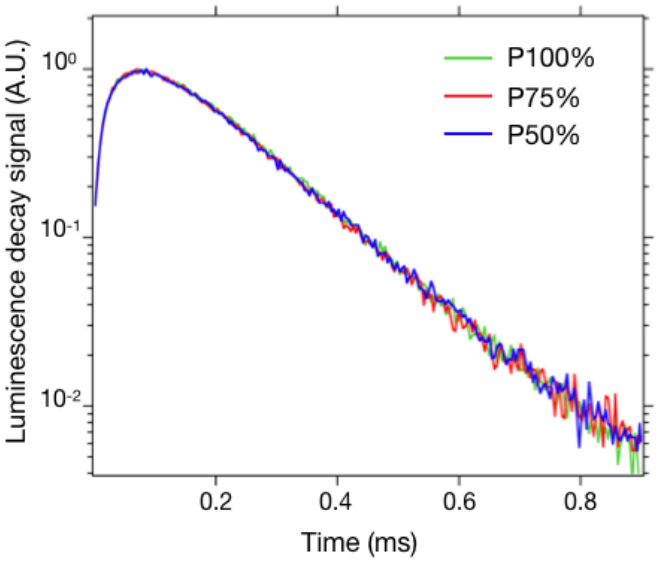

Figure S7. Lifetime decay curves from UCNPs coated with different HPS compositions at 0.1 mg/mL, namely, 100% St (green, P100%), 75% St: 25% MMA (red, P75%), 50% St: 50% MMA (blue, P50%). As observed from the plot, the lifetime decay curves of the resulting nanoparticles are very similar and seem independent of the HPS composition. This indicates that the tested range of shell compositions offer similar protection against the luminescence quenching caused by water molecules.

8. Integrated intensity of upconversion emissions from UCNPs-MDP, UCNPs-HPS and UCNPs-PAA.

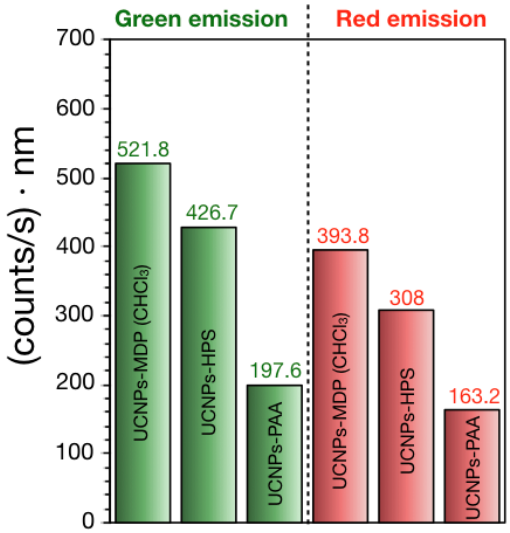

Figure S8. Steady state luminescence [(counts/s) nm] corresponding to the integration of the green ($^2H_{11/2}\rightarrow{}^4I_{15/2}$ and $^4S_{3/2}\rightarrow{}^4I_{15/2}$) and red ($^4F_{9/2}\rightarrow{}^4I_{15/2}$) emission bands of UCNPs with different coatings under CW 980 nm excitation (~100 W/cm^2). In all cases the UCNPs core concentration = 0.1 mg/mL. Left-green and left-red columns correspond to UCNPs-MDP in chloroform. Center-green and center-red columns correspond to UCNPs protected with HPS in water. Right-green and right-red columns correspond to UCNPs coated with PAA in water. The coating of UCNPs with HPS translates in a ~2.2-fold and a 1.9-fold improvement in their green and red emissions, respectively, in comparison with UCNP coated with PAA, highlighting the protective role of HPS from the quenching produced by water vibrational modes.

9. Theoretical luminescence decreases during UCNP degradation process.

We theoretically calculated the luminescence intensity as degradation of UCNPs-PAA in water at RT (control sample) takes place. The luminescence intensity was computed by considering the effect of the nanoparticle size decrease (showed by TEM images) on both, the number of active ions and the emission efficiency (or lifetime). First, the decrease of the nanoparticle radius r_{UC} leads to a reduction of the number of active ions which is proportional to the UCNP volume:

$$N_{Er} = \rho_{\mathrm{Er}} \frac{4\pi}{3} r_{UC}^3 \qquad (Eq.S9.1)$$

where N_{Er} and ρ_{Er} are the number and the concentration of Er^{3+} ions in the nanoparticle, respectively. Second, the decrease of the nanoparticle radius increases the surface area to volume ratio (S/V) which is well known to reduce the emission efficiency (or lifetime) due to surface quenching effects. We use the relationship between the luminescence lifetime and the S/V given by other works [4,5] to characterize the emission efficiency of the transitions involved in the upconversion mechanism, $\eta = \tau_f/\tau_{rad}$, where τ_{rad} is the corresponding radiative decay time. This relation is given by

$$\frac{1}{\tau_f} = 1600\ s^{-1} + 19000\ nm\ s^{-1}\ \frac{S}{V}(nm^{-1}) \qquad (Eq.S9.2)$$

Assuming that the red and green emission involved a two-step absorption process, the luminescence intensity is expected to depend on η quadratically. As expected, the luminescence intensity, calculated as $N_{Er}\eta^2$, properly reproduced the intensity drop when decreasing the UCNP diameter (see solid line in Figure S9). We also plotted in the same figure the contribution of the number of active ions N_{Er} (dashed line) to show that this intensity drop is mainly due to the ion dissolution so that the decrease in η with particle diameter only represents a small correction. Moreover, Figure S9 allowed us to predict that the variation of the UCNP size had a logarithmic relationship with time and that half of the reduction of the UCNP diameter took place during the first two-three hours. As stated before, the emission efficiency η exhibited a smaller variation with particle diameter (see dotted line in Figure S9).

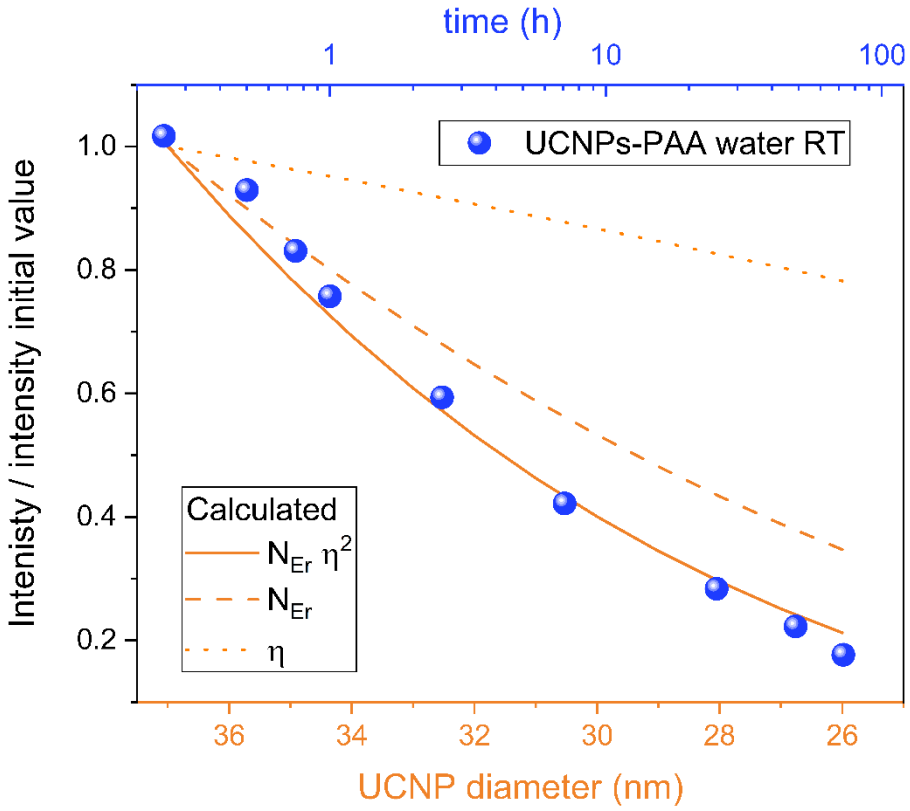

Figure S9. Experimental luminescence intensity normalized to its initial value as a function of time (circles). Theoretical luminescence intensity calculated from $N_{Er}\eta^2$ (solid line) or from N_{Er} (dashed line) normalized to its initial value as a function of particle diameter. We also plotted the variation of η (dotted line) as a function of particle diameter which gives the behavior of the luminescence decay time.

10. HAADF and elemental mapping analyses of UCNPs-PAA after 72 h in K^+PB.

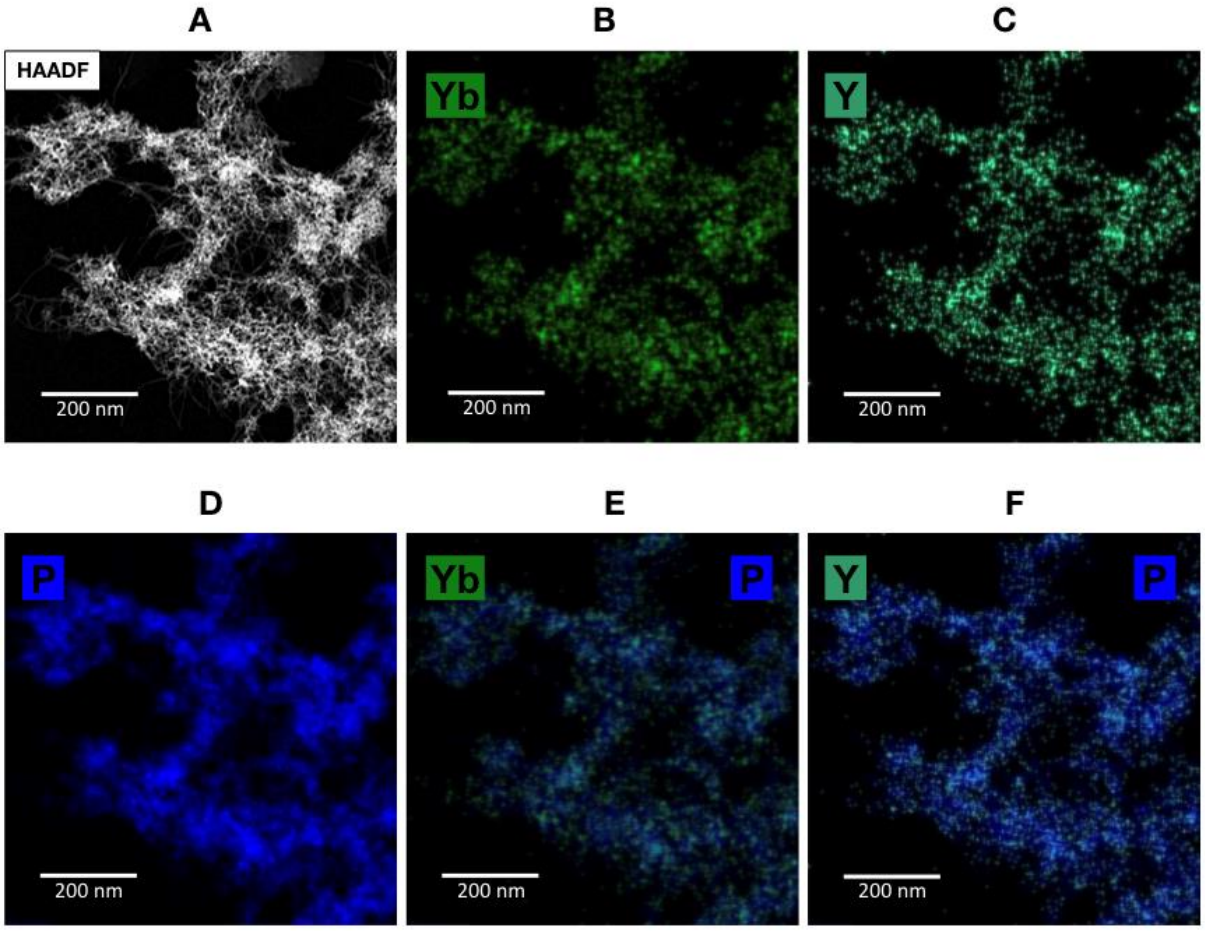

Figure S10. A) HAADF image of UCNPs-PAA after 72 h incubation in K^+PB. B), C), D), E) and F) are EDX elemental mapping analyses of UCNPs-PAA after 72 h incubation in K^+PB depicting signals from B) Ytterbium "Yb", C) Yttrium "Y", D) Phosphorus "P", E) merged Yb and P, and F) merged Y and P.

11. DLS of P100% and P75% in DI-H_2O and in K^+PB.

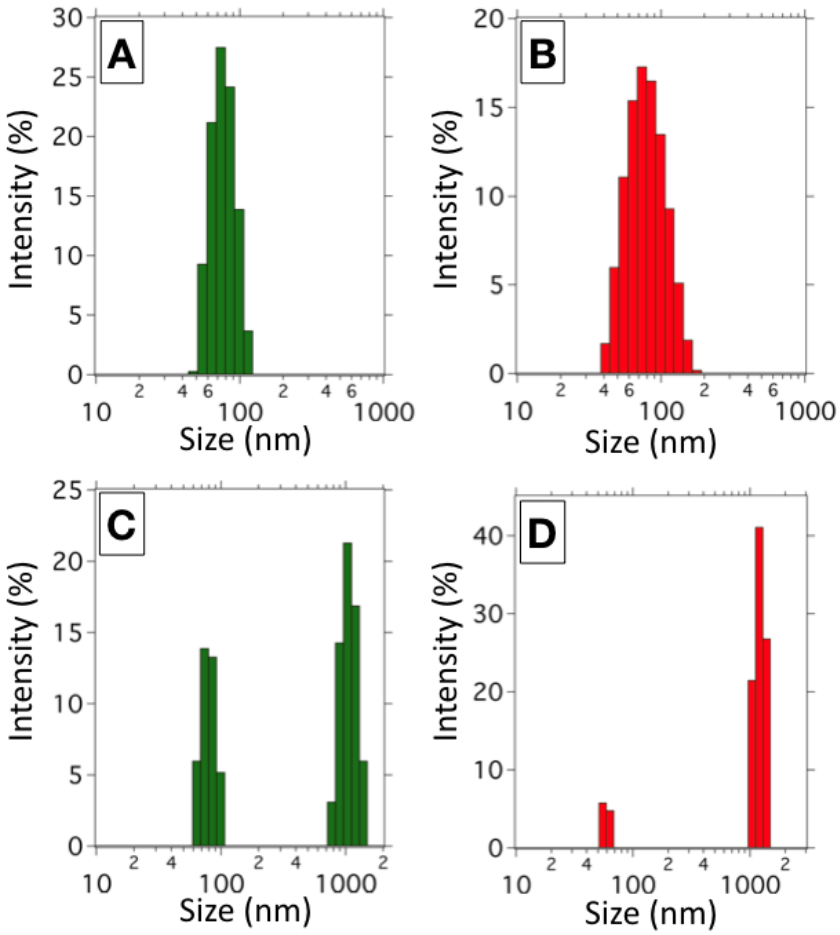

Figure S11. DLS analyses of P100% (green bars) and P75% (red bars). A) P100% in DI-H_2O; B) P75% in DI-H_2O; C) P100% in K^+PB; and D) P75% in K^+PB.

12. High magnification images of P100% and P75% after 72 h in K^+PB

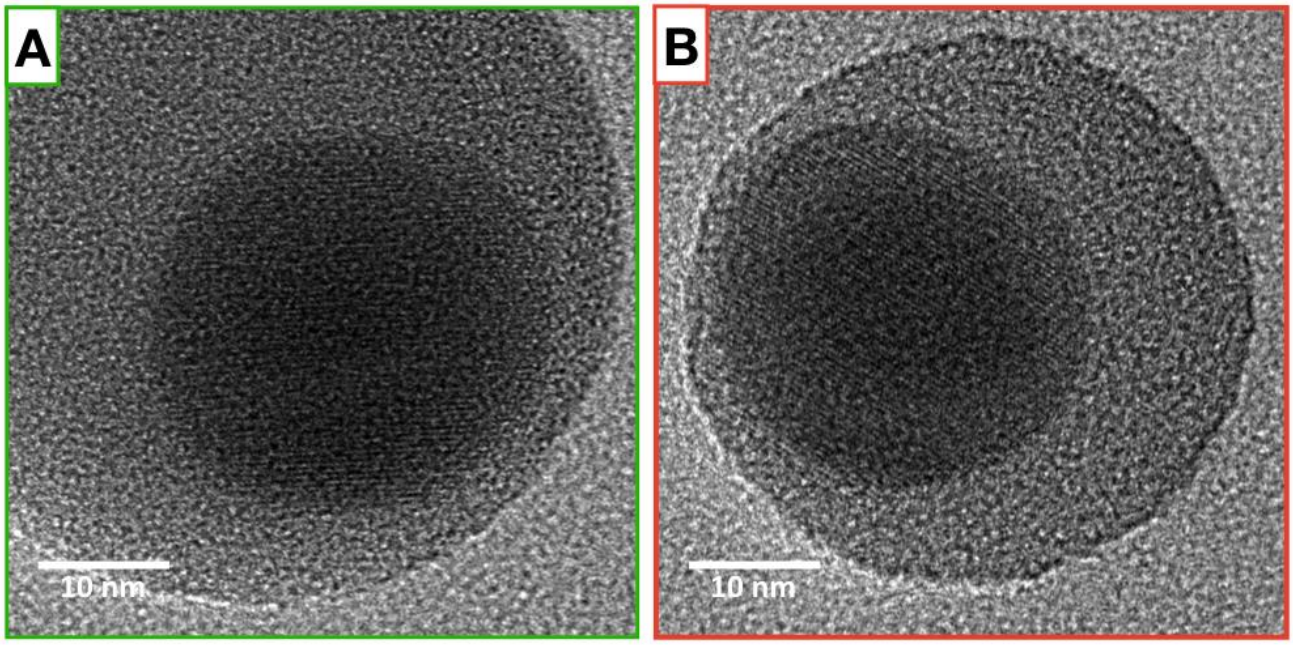

Figure S12. HR-TEM magnification of the UCNP core from A) P100%; and B) P75%; showing the β-$NaYF_4$:Yb:Er lattice planes after 72 h incubation in K^+PB.

13. Elemental mapping analyses of P75% before incubation in K^+PB

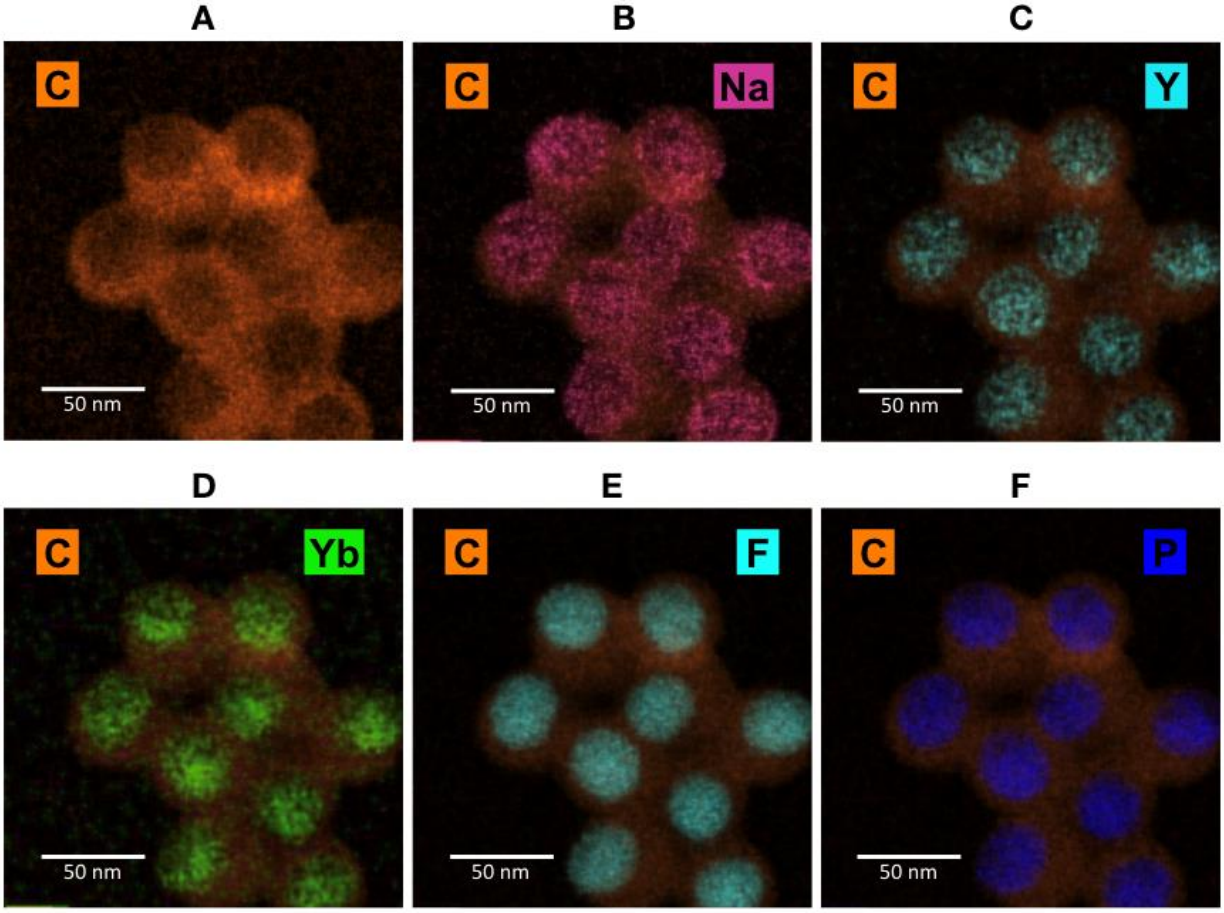

Figure S13. Elemental mapping analyses of P75% before incubation in K+PB showing signals from A) Carbon "C"; B) "C" and Sodium "Na"; C) "C" and Yttrium "Y"; D) "C" and Ytterbium; E) "C" and Fluoride "F"; F) "C" and Phosphorus "P".

14. Elemental mapping analyses of P100% and P75% after 72 h in K^+PB

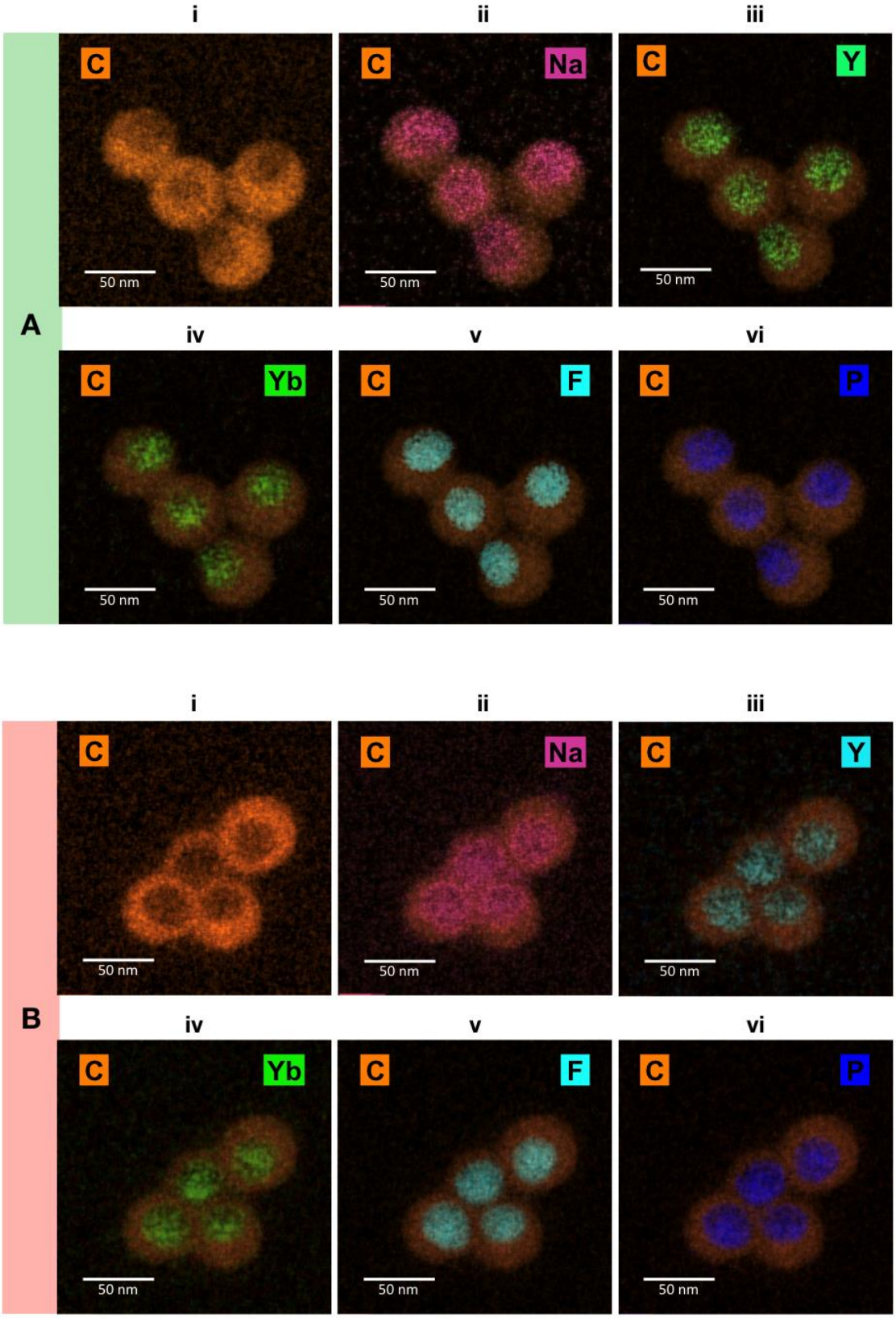

Figure S14. Elemental mapping analyses of A) P100% and B) P75% after 72 h incubation in K+PB. In both cases, elemental analyses correspond to i) Carbon "C"; ii) "C" and Sodium "Na"; iii) "C" and Yttrium "Y"; iv) "C" and Ytterbium; v) "C" and Fluoride "F"; vi) "C" and Phosphorus "P".

15. TEM images of P75% after 7 h at 70 ºC.

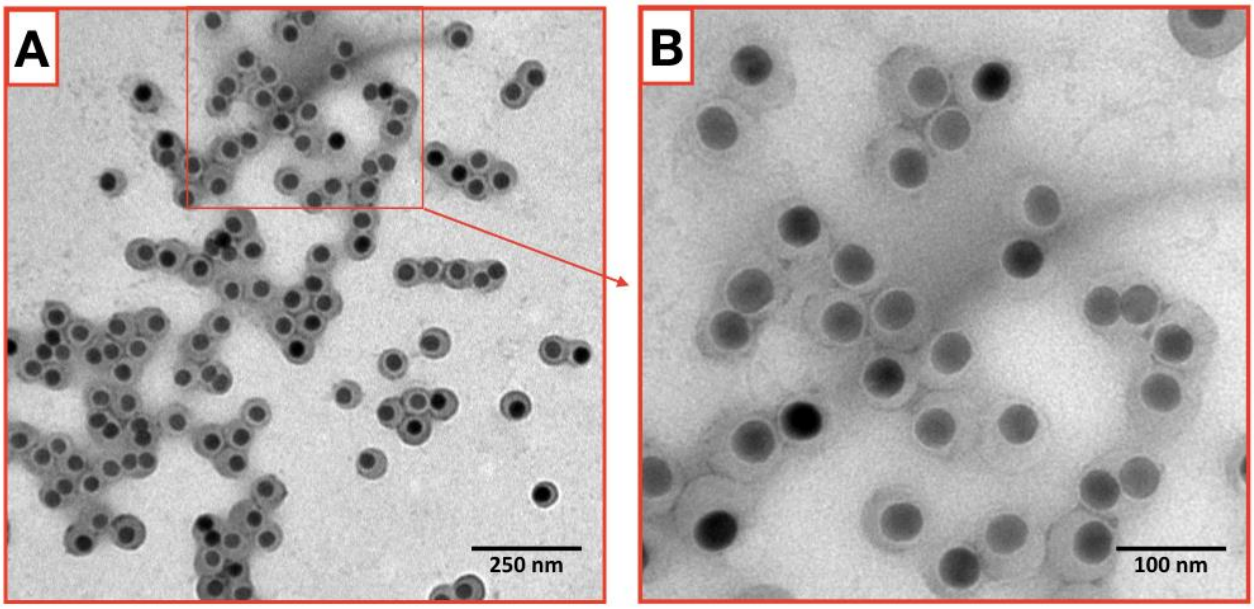

Figure S15. TEM images of P75% after 7 h at 70 ºC. A) General image. B) Image magnification from "A)".

16. List of Ln^{3+}-doped nanomaterials and host matrices potentially benefitting from HPS.

Table S2. The table reports some nanomaterials with a similar or lower K_{sp} than $NaYF_4$ that may benefit from their encapsulation into a hydrophobic polymer shell by enabling their protection in aqueous dispersion.

Material	K_{sp}	Reference
$NaYF_4$	1.60×10^{-26}	[6]
NH_4ScF_4	2.55×10^{-12}	[7]
$CaWO_4$	$8.70 \times x10^{-9}$	[8]
YF_3	3.98×10^{-19}	[9,10]
LaF_3	3.26×10^{-21}	[7,10]
LuF_3	1.26×10^{-19}	[7,11]
ScF_3	2.98×10^{-12}	[7,10]

17. References

[1] D. Olmos, E. V. Martín, and J. González-Benito. “New molecular-scale information on polystyrene dynamics in PS and PS–$BaTiO_3$ composites from FTIR spectroscopy” Phys. Chem. Chem. Phys., 2014, 16, 24339-24349.

[2] Stoil Dirlikov, Jack L. Koenig. “Infrared Spectra of Poly(Methyl Methacrylate) Labeled with Oxygen-18” Applied Spectroscopy, 1979, 33, 6, 551-555

[3] Guorong Duan, Chunxiang Zhang, Aimei Li, Xujie Yang, Lude Lu & Xin Wang. “Preparation and Characterization of Mesoporous Zirconia Made by Using a Poly (methyl methacrylate) Template” Nanoscale Research Letters, 2008, 3, 118-122.

[4] Xiaojie Xue, Shinya Uechi, Rajanish N. Tiwari, Zhongchao Duan, Meisong Liao, Masamichi Yoshimura, Takenobu Suzuki, and Yasutake Ohishi. "Size-dependent upconversion luminescence and quenching mechanism of $LiYF_4:Er^{3+}/Yb^{3+}$ nanocrystals with oleate ligand adsorbed" Opt. Mater. Express, 2013, 3, 989-999

[5] Shuang Fang Lim, William S. Ryu, and Robert H. Austin. "Particle size dependence of the dynamic photophysical properties of $NaYF_4$:Yb,Er nanocrystals" Opt. Express, 2010, 18, 2309-2316

[6] Sandy F. Himmelstoss and Thomas Hirsch. “Long-Term Colloidal and Chemical Stability in Aqueous Media of $NaYF_4$-Type Upconversion Nanoparticles Modified by Ligand-Exchange” Part.Part. Syst. Charact. 2019, 36, 1900235

[7] D. Lisjak, O. Plohl, M. Ponikvar-Svet, and B. Majaron. “Dissolution of upconverting fluoride nanoparticles in aqueous solutions” RSC Adv. 2015, 5, 27393-27397

[8] Chunyan Liu, Zhenyu Gao, Jianfeng Zeng, Yi Hou, Fang Fang, Yilin Li, Ruirui Qiao, Lin Shen, Hao Lei, Wensheng Yang, and Mingyuan Gao. “Magnetic/Upconversion Fluorescent $NaGdF_4$:Yb,Er Nanoparticles-Based Dual-Modal Molecular Probes for Imaging Tiny Tumors in Vivo” ACS Nano, 2013, 7, 7227-7240

[9] Oleksii Dukhno, Frederic Przybilla, Verena Muhr, Markus Buchner, Thomas Hirsch and Yves Mely. “Time-dependent luminescence loss of individual upconversion nanoparticles upon dilution in aqueous solutions” Nanoscale, 2018, 10, 15904-15910

[10] Tomasz Mioduski, Cezary Gumiski, and Dewen Zeng. “IUPAC-NIST Solubility Data Series. 100. Rare Earth Metal Fluorides in Water and Aqueous Systems. Part 1. Scandium Group (Sc, Y, La)” J. Phys. Chem. Ref. Data, 2014, 43, 013105

[11] Tomasz Mioduski, Cezary Gumiski, and Dewen Zeng. “IUPAC-NIST Solubility Data Series. 100. Rare Earth Metal Fluorides in Water and Aqueous Systems. Part 3. Heavy Lanthanides (Gd-Lu)” J. Phys. Chem. Ref. Data, 2015, 44, 023102